

1 **A Froude-scaled model of a bedrock-alluvial channel reach: 2. Sediment cover**

2 **Rebecca A. Hodge¹ & Trevor B. Hoey²**

3 ¹ Department of Geography, Durham University, UK

4 ² School of Geographical and Earth Sciences, University of Glasgow, UK

5 **Key points:**

6 1. Sediment patches tend to form in low elevation, sheltered, areas, but high flow velocities
7 can override this

8 2. At lower sediment supply, bed topography determines patch stability and patches are
9 relatively insensitive to sediment supply

10 3. At higher sediment supply, sediment patches stabilise by grain-grain and grain-flow
11 interactions

12

13 **Abstract**

14 Previous research into sediment cover in bedrock-alluvial channels has focussed on total
15 sediment cover, rather than the spatial distribution of cover within the channel. The latter is
16 important because it determines the bedrock areas that are protected from erosion, and the
17 start and end of sediment transport pathways. We use a 1:10 Froude-scaled model of an 18 by
18 9 m reach of a bedrock-alluvial channel to study the production and erosion of sediment
19 patches, and hence the spatial relationships between flow, bed topography and sediment
20 dynamics. The hydraulics over this bed are presented in the companion paper. In these
21 experiments specified volumes of sediment were supplied at the upstream edge of the model
22 reach as single inputs, at each of a range of discharges. This sediment formed patches and,
23 once these stabilised, flow was steadily increased to erode the patches. In summary: 1)
24 patches tend to initiate in the lowest areas of the bed, but areas of topographically-induced
25 high flow velocity can inhibit patch development; 2) at low sediment inputs the extent of
26 sediment patches is determined by the bed topography and can be insensitive to the exact
27 volume of sediment supplied; and, 3) at higher sediment inputs more extensive patches are
28 produced, stabilised by grain-grain and grain-flow interactions, and less influenced by the bed
29 topography. Bedrock topography can therefore be an important constraint on sediment patch
30 dynamics, and topographic metrics are required that incorporate its within-reach variability.
31 The magnitude and timing of sediment input events controls reach-scale sediment cover.

32 **1. Introduction**

33 The spatial pattern of sediment cover in a bedrock-alluvial river is important in a range of
34 different contexts. First, sediment cover protects the bed from erosion; the pattern of cover
35 determines which parts of the bed are exposed to erosive processes, and therefore has
36 implications for incision rates and landscape evolution [*Sklar and Dietrich, 2004; Johnson*
37 *and Whipple, 2010*]. Secondly, tracer experiments in a bedrock-alluvial channel demonstrate
38 that grain travel paths are predominantly from one sediment patch to the next [*Hodge et al.,*
39 *2011*]. Analogous to the role of riffles and pools in alluvial systems [e.g. *Pyrce and Ashmore,*
40 *2003*], the spatial pattern of sediment patches in bedrock-alluvial channels determines grain
41 transport distances, as grains are preferentially deposited in sediment patches. Thirdly, the
42 contrast between alluvial and bedrock areas affects the critical shear stress for grain
43 entrainment and consequently sediment transport [*Goode and Wohl, 2010; Hodge et al.,*
44 *2011*]. Finally, both the spatial arrangement and stability of areas of sediment cover affect
45 instream biota and these areas are potentially of greater ecological importance than
46 continuous alluvial sediments [*O'Connor et al., 2014*]. This paper reports the use of a
47 Froude-scaled physical model of a specific bedrock-alluvial channel to analyse the factors
48 that control the spatial pattern and stability of sediment cover. This is the second in a pair of
49 papers; the companion paper demonstrates the Froude scaling of the model, and quantifies
50 relationships between the bed topography and hydraulics.

51 **2. Background and Research Questions**

52 Field observations [*Hodge et al., 2011*], flume experiments [*Chatanantavet and Parker,*
53 *2008; Hodge et al. 2016*] and theoretical analyses [*Hodge et al., 2011; Nelson and Seminara,*
54 *2012; Nelson et al., 2014*] have demonstrated that the most stable configuration of sediment

55 on a bedrock surface is in patches, producing a spatial pattern of discrete alluvial and bedrock
56 areas. Despite this, within-reach scale patterns of sediment cover in bedrock-alluvial rivers
57 have not received significant attention. From the perspective of incision and landscape
58 evolution the focus has been on the total amount of sediment cover [e.g. *Sklar and Dietrich*,
59 2004; *Nelson and Seminara* 2012; *Lague*, 2014], but not where that cover occurs within the
60 channel. The rationale for this focus is that, over long time periods, there is negative feedback
61 between local channel elevation, sediment cover and erosion, and therefore the bedrock
62 incision and the locations of sediment cover will be averaged out across the reach; in this case
63 the details at shorter timescales are unimportant. However, other flume experiments [e.g.
64 *Johnson and Whipple*, 2007; *Finnegan et al.*, 2007] have demonstrated positive feedback
65 between the location of sediment and channel incision, in which case the spatial pattern of
66 sediment cover could be important in determining the long term morphological evolution.
67 The first step in understanding these feedbacks, and evaluating the importance of within-
68 reach scale patterns, is to understand the controls on the location and stability of sediment
69 cover.

70 Although incision models retain a reach-averaged focus, they increasingly include grain-scale
71 processes. The grain-scale processes are often directly upscaled to the reach-scale, ignoring
72 the sub-reach scale complexities of these systems [*Lague*, 2014]. Such grain-scale processes
73 include grain saltation [*Sklar and Dietrich*, 2004], suspension [*Lamb et al.*, 2008; *Scheingross*
74 *et al.*, 2014], the impact of grain-grain interactions on entrainment [*Hodge and Hoey*, 2012],
75 the impact of differences in roughness between bedrock and alluvial surfaces on sediment
76 cover [*Nelson and Seminara*, 2012; *Johnson*, 2014; *Inoue et al.*, 2014], the impact of surface
77 topographies on both sediment cover [*Chatanantavet and Parker*, 2008] and grain impact
78 trajectories and hence erosion rates [*Huda and Small*, 2014]. However, many of these
79 processes will also be affected by the pattern of sediment cover within a reach; for example,
80 saltation trajectories will be affected by the mixture of bedrock and alluvial surfaces that a
81 saltating grain travels across, and channel roughness will vary spatially depending on the
82 local bed morphology and sediment cover.

83 This paper uses a Froude-scaled model of a reach of a bedrock river to analyse the formation
84 and erosion of sediment patches formed by discrete sediment pulses, and to assess the extent
85 to which these processes vary with sediment mass, discharge and local bed topography. Our
86 research questions are:

- 87 1. How does the amount of sediment cover vary with flow discharge and supplied
88 sediment mass?
- 89 2. To what extent does bed topography control: a) sediment patch location; and, b) patch
90 stability?
- 91 3. What are the relationships between sediment patch occurrence, hydraulics and local
92 bed topography?

93
94 The model was created using a novel combination of Terrestrial Laser Scanning (TLS) and
95 3D printing. This model is Froude-scaled, which is an advance over previous models of
96 bedrock-alluvial channels that have had Froude numbers significantly higher than are found

97 in many bedrock channels [*Chatanantavet and Parker, 2008; Johnson and Whipple, 2010*].
98 Furthermore, the dimensions of the model (0.9 m wide) mean that spatially distributed
99 hydraulics can be measured, and these data are presented in the companion paper [*Hodge and*
100 *Hoey, in review*]. Although these hydraulic data are mostly independent of the data presented
101 here, they provide a useful approximation for the hydraulic conditions in these experiments;
102 here rapidly changing flow and sediment cover prevented the collection of spatially
103 distributed hydraulic data. The focus of our experiments is also different from previous
104 physical models. *Chatanantavet and Parker [2008]* analysed sediment cover from a reach-
105 averaged perspective, considering the total amount of sediment cover, with only qualitative
106 descriptions of where on the bed that sediment cover was developing. *Finnegan et al. [2007]*
107 and *Johnson and Whipple [2007]* addressed the interactions between sediment cover and an
108 eroding topography. Here a static topography is used, meaning that bed topography is
109 independent of sediment and flow parameters.

110

111 **3. Methods**

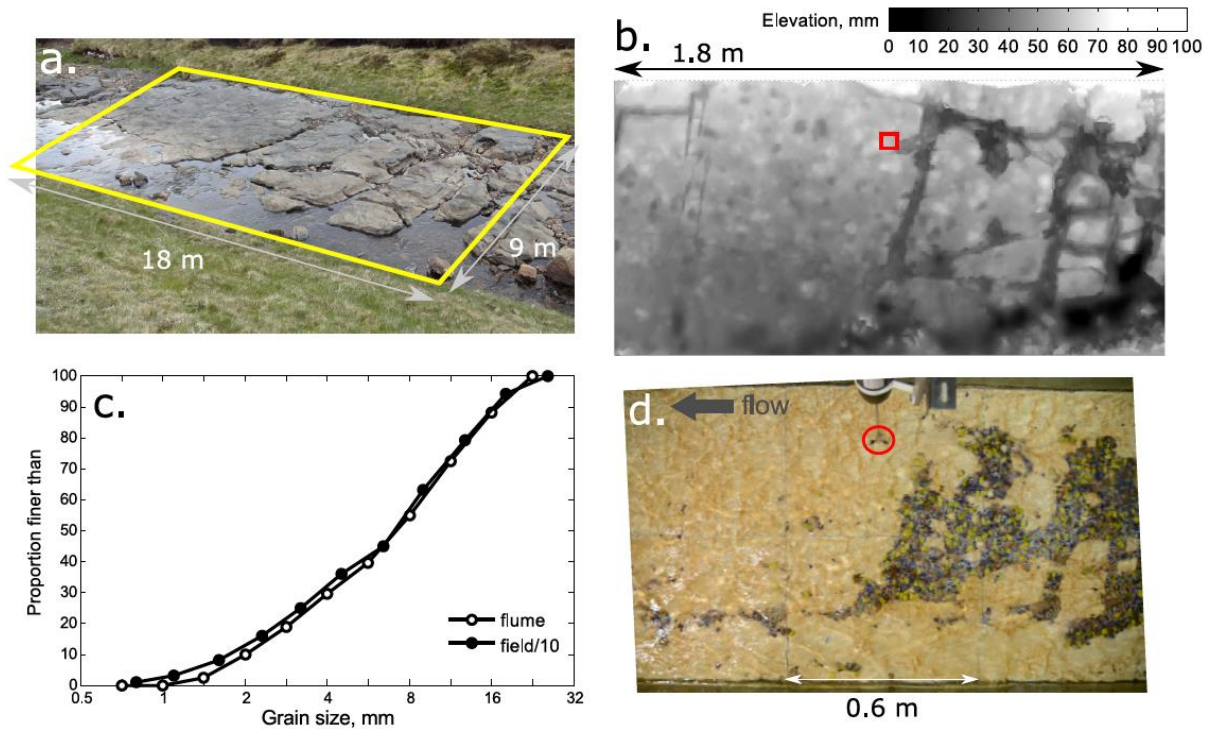
112 **3.1. Field and Flume Methods**

113 The reach reproduced in the flume is an 18 m long section of Trout Beck, North Pennines, UK
114 ($54^{\circ}41'35''\text{N } 2^{\circ}23'18''\text{W}$), which has an average width of 9 m, gradient of 0.02, and 22%
115 sediment cover. The bedrock is Alston Formation Limestone, and the channel bed has a
116 blocky topography with approximately horizontal bedding ~ 0.5 m thick, preferential erosion
117 along vertical joints, vertical relief of up to 1 m and a standard deviation of surface elevations
118 of 0.12 m. (Figure 1a). Although the study reach does not have the extreme topography of
119 some bedrock-alluvial channels, its topography is representative of many other channels (e.g.
120 images in *Tinkler and Wohl, 1998; Inoue et al., 2014; and Whitbread et al., 2015*). Sediment
121 has a D_{16} , D_{50} and D_{84} of 23, 70 and 146 mm, respectively (where D_x is the grain size for
122 which $x\%$ is finer; grain-size distribution shown in Figure 1c).

123 Terrestrial laser scanning, supplemented by differential GPS surveying of submerged areas of
124 the bed, and 3D printing were used to create a 1:10 Froude scaled model of this reach of
125 Trout Beck in the 8 m working length, 0.9 m wide flume at the University of Glasgow
126 (Figure 1b and d). It was not feasible to remove the 22% sediment cover prior to surveying
127 the reach, but this cover is mostly only a single grain thick. The presence of sediment cover
128 indicates that this is a suitable reach for recreating sediment cover in the flume. The flume
129 experiments indicate where additional sediment inputs to this channel would be deposited,
130 but because of the different initial conditions, the experimental sediment patch locations
131 cannot be compared to those in the channel. The printed surfaces, comprising 6 individual
132 tiles, were installed in the flume 3.5 m downstream from the inlet, and the rest of the flume
133 was filled with sediment of a comparable roughness to the printed bed. Full details of the
134 model creation, and a comparison of flume and field data that demonstrates the Froude
135 scaling, are presented in the companion paper [*Hodge and Hoey, in review*].

136 Two sets of experiments were performed, focussing on hydraulics and sediment, respectively.
137 In the first set [reported in the companion paper, *Hodge and Hoey, in review*], 3D velocity
138 data were collected from each of 18 locations, at discharges ranging from 20 to 60 l s^{-1} . These

139 data show that hydraulic properties become more spatially variable as discharge increases,
 140 and that a core of super-critical flow develops along the model domain. The hydraulic data
 141 from these 18 measurement locations give the following mean values and standard errors: Fr
 142 [0.88 ± 0.016 at $Q = 20 \text{ l s}^{-1}$ to 1.09 ± 0.019 at $Q = 60 \text{ l s}^{-1}$]; (h/D_{84}) [2.74 ± 0.050 to $4.74 \pm$
 143 0.054]; f [3.80 to 0.97]; and τ^* [0.067 ± 0.0012 to 0.116 ± 0.0013]. In these calculations,
 144 reach-averaged slope, S_l , has been used, Fr = Froude number, h = flow depth, f = Darcy-
 145 Weisbach roughness coefficient, and $\tau^* = (hS_l/1.65D_{50})$, assuming water and sediment
 146 densities of 1000 kg m^{-3} and 2650 kg m^{-3} , respectively.



147
 148 *Figure 1: a) The field location that was reproduced in the flume. b) 1:10 scale digital*
 149 *elevation model of the field reach bed topography created from terrestrial laser scanning and*
 150 *differential GPS data. c) Grain size distributions for the field and flume sediment. Field data*
 151 *are downscaled by a factor of 10. d) An image of the flume bed from run Q20/S16 (initial*
 152 *discharge of 20 l s^{-1} , 16 kg sediment pulse), showing sediment cover. The coloured grains*
 153 *correspond to D_{16} , D_{50} and D_{84} . The 0.6 m arrow indicates the width of one printed tile. The*
 154 *location of the Acoustic Doppler Velocimeter is circled in d) and the area in which velocities*
 155 *and sediment cover were measured is the red square in b).*

156 In the second set of experiments (reported here), over a range of initial discharges, individual
 157 sediment pulses were introduced at the upstream end of the modelled reach so that the
 158 sediment formed sediment patches. Patch stability was then assessed by gradually increasing
 159 the discharge. These sediment experiments used a 1:10 scaled version of the field sediment,
 160 truncated at 1 mm, with D_{16} , D_{50} and D_{84} of 2.6, 7.3 and 14.8 mm, respectively and
 161 subrounded grains. Only 4% of the original 1:10 scale grain size distribution was smaller than
 162 1 mm (Figure 1c). In each run, the discharge was initially stabilised at a constant value, a
 163 specified quantity of sediment was input in a single pulse at the upstream end of the printed
 164 flume bed (using a board to disperse sediment evenly across the flume) and sediment patches

165 formed. Five minutes after the sediment input, the discharge began to be increased at a rate of
166 0.7 l min^{-1} until a maximum discharge of 75 l s^{-1} (maximum pump capacity) was reached.
167 Two sets of data were collected during each run; a downward-facing SLR camera took an
168 image of the bed every 5 seconds, and 3D acoustic Doppler velocimetry (ADV) data were
169 collected at 25 Hz from a fixed location in the flume (Figure 1d). The ADV data show the
170 impact of sediment cover on local hydraulics, and are analysed in the companion paper.

171 The sediment experiments used three different initial discharges (20, 35 and 50 l s^{-1} , denoted
172 Q) and four different sediment masses (2, 4, 8 and 16 kg, denoted S) in the following
173 combinations: Q20/S0, Q20/S2, Q20/S4, Q20/S8, Q20/S16, Q35/S4, Q35/S8, Q35/S16,
174 Q50/S2, Q50/S4, Q50/S8. The range of sediment masses and discharges was selected to
175 cover a range of field conditions (20 l s^{-1} is equivalent to just below bankfull in the field
176 setting) and to produce a range of sediment cover extents. Three further runs at Q20/S4 were
177 completed; one replicate with the same sediment (Q20/S4_{rep}), one with coarse angular
178 uniform 16 mm sediment (Q20/S4_C) and one with fine angular uniform 8.5 mm sediment
179 (Q20/S4_F). The uniform sediment runs allowed the impact of sediment sorting and shape to
180 be assessed, and comparison with experiments presented in *Hodge et al.* [2016] which
181 quantified the stability of sediment patches of this uniform sediment on a flat bed, allows
182 assessment of the impact of the rougher topography in these experiments. Experimental
183 duration was determined by the rate of changing discharge, and ranged from 33 min to 85
184 min for experiments starting at 50 l s^{-1} and 20 l s^{-1} , respectively.

185 Camera images were processed in Matlab to segment automatically the sediment patches
186 from the background, and thus produce a map of sediment cover. The segmentation technique
187 used the red channel in the RGB image as this had the greatest contrast between the bed and
188 sediment. First, a background model from initial images of the flume bed without sediment
189 cover was produced by averaging 12 images. Sediment was then identified as areas where the
190 pixel values decreased relative to the background model. The background model was updated
191 to account for changes in water depth throughout each experiment. Further filtering removed
192 noise caused by the water surface. A video of run Q20/S16 (Movie S1) shows the results of
193 the segmentation algorithm and the dynamics of an experimental run. Errors associated with
194 changes in pixel location produced by refraction at different water depths were minimal
195 compared to other segmentation errors, and were not corrected for.

196 Sediment cover maps were produced at one minute intervals for each run. The segmentation
197 algorithm was tested through comparison with a total of 28 manually segmented images,
198 comprising up to 10 images from each of three runs (Q20/S2, Q20/S8 and Q20/S16). The
199 Jaccard index (J) was used to calculate the similarity between the manual and automatic
200 segmentation, where the index of two areas, A (manually segmented sediment) and B
201 (automatically identified sediment), is:

$$202 \quad J(A,B) = \frac{|A \cap B|}{|A \cup B|} \quad (1)$$

203 J accounts for the location as well as the amount of sediment cover. Values range between 0
204 and 1; values closer to one indicating a higher correlation between the two images. The mean

205 (and range) of J values for each set of images from a flume run are: Q20/S2, 0.68 (0.62 to
206 0.77); Q20/S8, 0.76 (0.70 to 0.84) and Q20/S16, 0.84 (0.74 to 0.91). Much of the
207 dissimilarity between the manual and automated segmentations occurs around patch edges
208 and in small patches which are either missed or erroneously identified by the manual
209 segmentation. Consequently, J values are higher when there is more sediment cover because
210 these errors comprise a smaller proportion of the total area. For further illustration, absolute
211 differences between manual and automatically segmented sediment cover range from 0.1 to
212 2.4 % of the total image area, with a root mean square (RMS) error of 0.9%, and tend to
213 decrease as sediment cover decreases.

214 Images and sediment cover maps were registered to a common coordinate system using a
215 series of 12 markers on the tiles; the RMS of the registration errors was 6.4 mm. This enables
216 sediment cover to be correlated with bed topography. Sediment cover maps and the bed
217 topography model were resampled onto a 5 mm grid to ensure comparable and spatially
218 uniform datasets. A time-discharge rating curve was used to calculate the discharge in the
219 flume during each of the sediment cover maps.

220 The final component of the methods is a simple numerical model designed to provide a
221 control condition in which patches develop independent of any interaction with the flow.
222 Such an approach has been used to estimate reach-scale sediment cover [Inoue *et al.*, 2015].
223 This space filling model determines the sediment cover produced by filling up the channel
224 bed topography. The cells of the digital elevation model were virtually filled, starting from
225 the lowest cell and adding cells in order of increasing elevation. Throughout the process, the
226 sediment surface elevation was the same in all sediment-containing cells; this assumption is
227 not necessarily true in the field and flume. Filling continued until the volume of virtual
228 sediment was equal to a specified mass (assuming a density of 2.65 g cm^3 and porosity of
229 0.3).

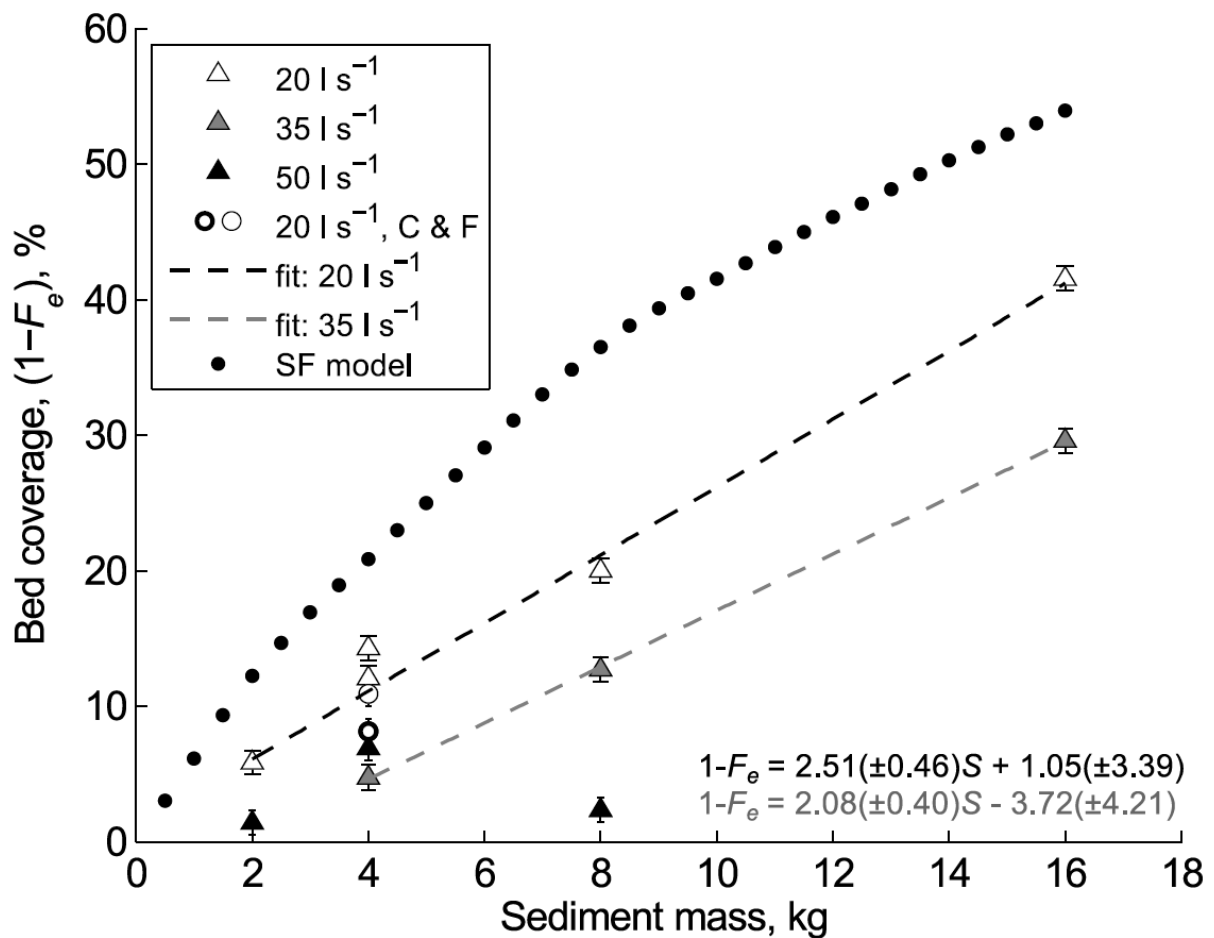
230 **4. Results**

231 **4.1. The extent and spatial pattern of initial sediment cover**

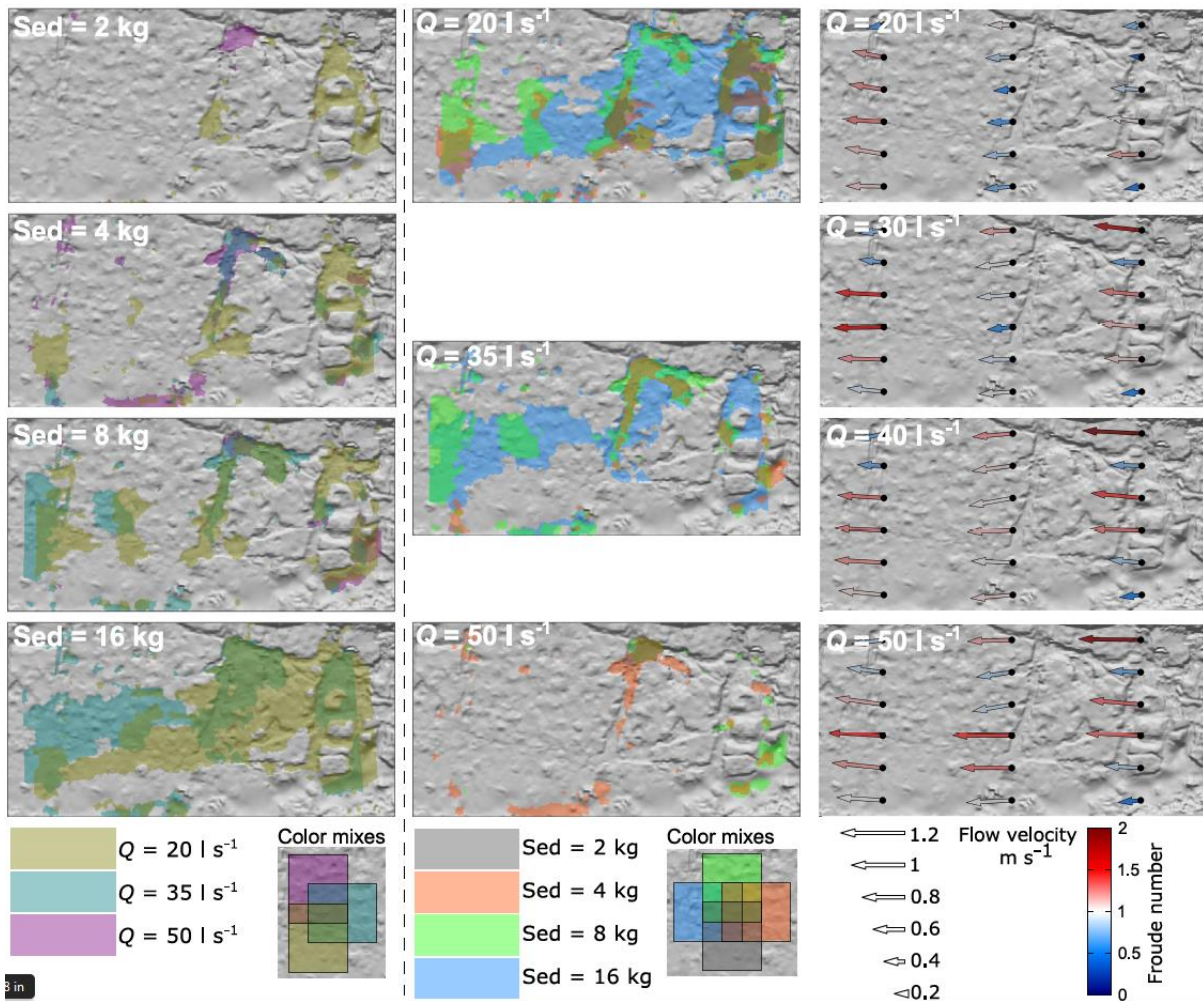
232 Initial patterns of sediment cover are analysed 4.5 minutes after the sediment injection, prior
233 to the subsequent increase in flow. Figure 2 shows linear relationships between the proportion
234 of the flume bed covered by sediment and the mass of sediment that was added to the flume
235 for both $Q = 20 \text{ l s}^{-1}$ and $Q = 35 \text{ l s}^{-1}$. At 50 l s^{-1} , transport was more intense and less sediment
236 was retained in the modelled section. The latter experiments do not follow a linear
237 relationship due to an anomalously high cover in run Q50/S4 which may be the result of the
238 backwater from the flume tailgate extending up to the downstream end of the tiles in this run.

239 For $Q = 20 \text{ l s}^{-1}$, $Q = 35 \text{ l s}^{-1}$, and for all data combined, the gradients of the relationships
240 between sediment mass and cover are not significantly different (95% confidence; see Figure
241 2 for values). There is systematic variation in the intercept (albeit not at a 95% confidence
242 interval), which results in higher discharges producing lower cover. Stepwise regression of
243 cover against sediment mass and discharge indicate that both significantly contribute to the
244 relationship, with respective p-values of < 0.001 and 0.003 . The initial sediment cover in the
245 runs with uniform coarse and fine sediment (Q20/S4_C and Q20/S4_F) was 8.1 and 10.9%,

246 respectively, which is consistent with the trend of the $Q = 20 \text{ l s}^{-1}$ runs; adding or removing
 247 these data makes no significant difference to the regression in Figure 2.



248
 249 *Figure 2: Percentage of bed with sediment cover ($1 - F_e$, where F_e is bedrock exposure) at*
 250 *4.5 minutes after sediment input into the flume. Circles are coarse and fine uniform*
 251 *sediments. Error bars are the 0.9% root mean square error between manual and automated*
 252 *segmentations. Black dots are predictions of sediment cover from an elevation-based space*
 253 *filling model. Linear regressions fitted to data are as follows, where S is sediment mass: all*
 254 *data: $1 - F_e = 2.11(\pm 0.81)S - 0.54(\pm 6.38)$, $R^2 = 0.75$; $Q = 20 \text{ l s}^{-1}$ (including coarse and fine*
 255 *sediment): on figure, $R^2 = 0.98$; $Q = 35 \text{ l s}^{-1}$: on figure, $R^2 = 0.99$. Stepwise regression of*
 256 *sediment mass and discharge against sediment cover, for all mixed sediment size*
 257 *experiments, gives: $1 - F_e = 2.07S - 0.34Q + 10.20$, $R^2 = 0.88$.*



259

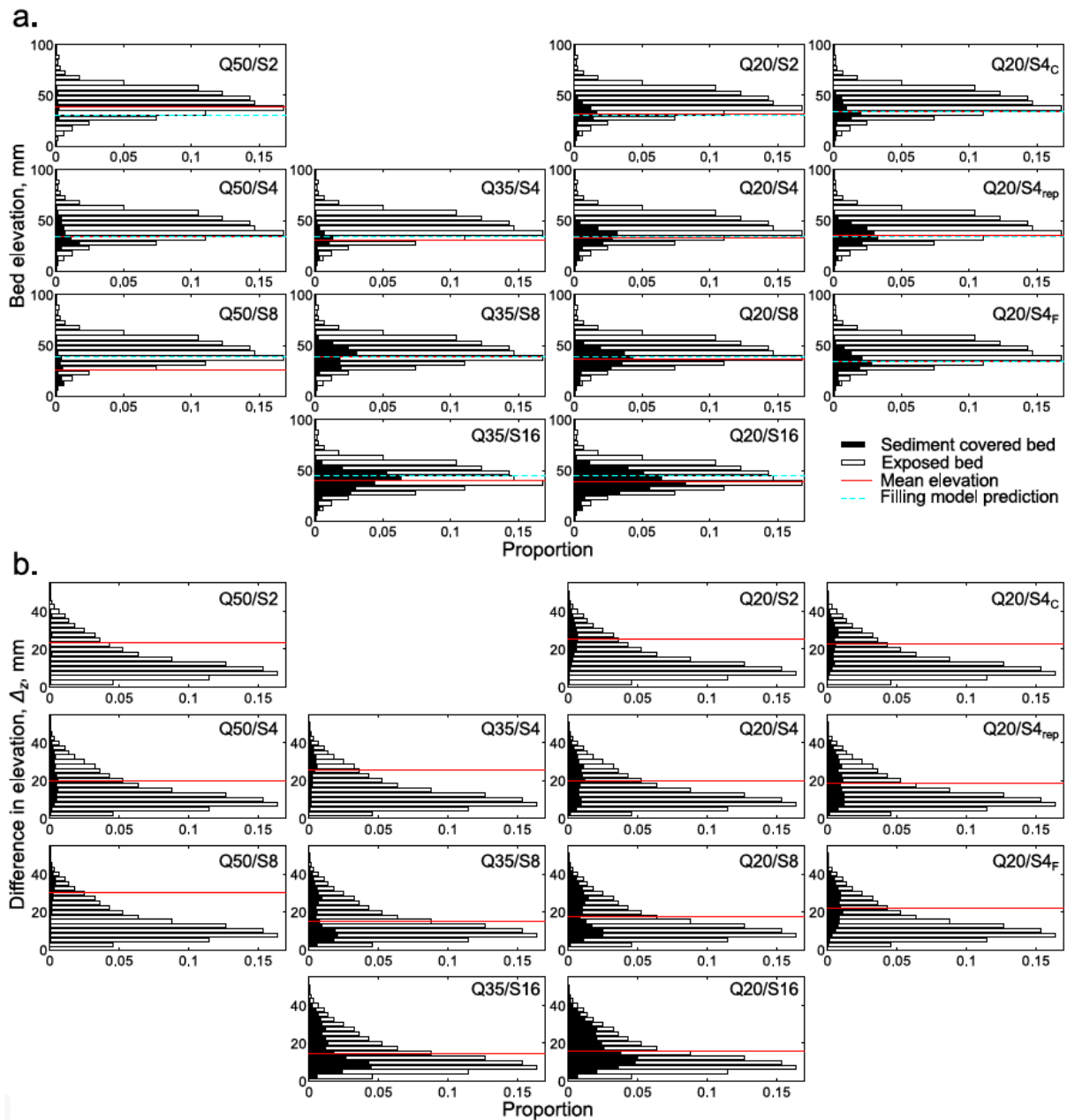
260 *Figure 3: Overlays of initial sediment cover for runs with the same sediment mass (left) or*
 261 *same initial discharge (middle). Colours are transparent, so mixture panels show how the*
 262 *colours combine. Data are for all runs with mixed sediment sizes. Bed area is 1.8 m long by*
 263 *0.9 m wide. Sediment patches are truncated within about 50mm of upstream and/or*
 264 *downstream ends because the photos did not cover the entire length of the test section. Flow*
 265 *velocities and Froude numbers measured at 18 locations across the flume are also shown for*
 266 *a range of discharges (right, see companion paper Hodge and Hoey [in revision] for further*
 267 *details). Note that the velocity data were collected with no sediment in the flume, therefore*
 268 *are only illustrative of the conditions during the sediment runs.*

269 Despite the differences in sediment mass and discharge, there are similarities between the
 270 locations of sediment cover (Figure 3); 47.5% of the flume bed area never had initial
 271 sediment cover, whereas 1.2% had initial sediment cover in at least 10 out of the 13
 272 experiments. For runs with the same initial discharge but different sediment masses, there is
 273 persistence in the location of the initial sediment patches. For almost all runs, at least 70% of
 274 the locations that are initially sediment covered in one run also have sediment cover in
 275 subsequent runs with higher sediment masses but the same initial discharge. The main
 276 differences in sediment location are caused by changes in initial discharge. At initial
 277 discharges of 20 and 35 l s^{-1} , sediment patches form in low elevation areas at the upstream

278 end of the reach. However, at an initial discharge of 50 l s^{-1} , sediment is preferentially
 279 deposited in depressions further downstream. Figure 3 shows how velocities in the upstream
 280 transect increased at high discharges, inhibiting sediment deposition. Furthermore, sediment
 281 was introduced to the flume $<0.3\text{m}$ upstream of these areas, and at higher discharges would
 282 have acquired a larger downstream velocity so overpassing the upstream areas of the bed.

283 4.2. Topographic controls on initial sediment cover

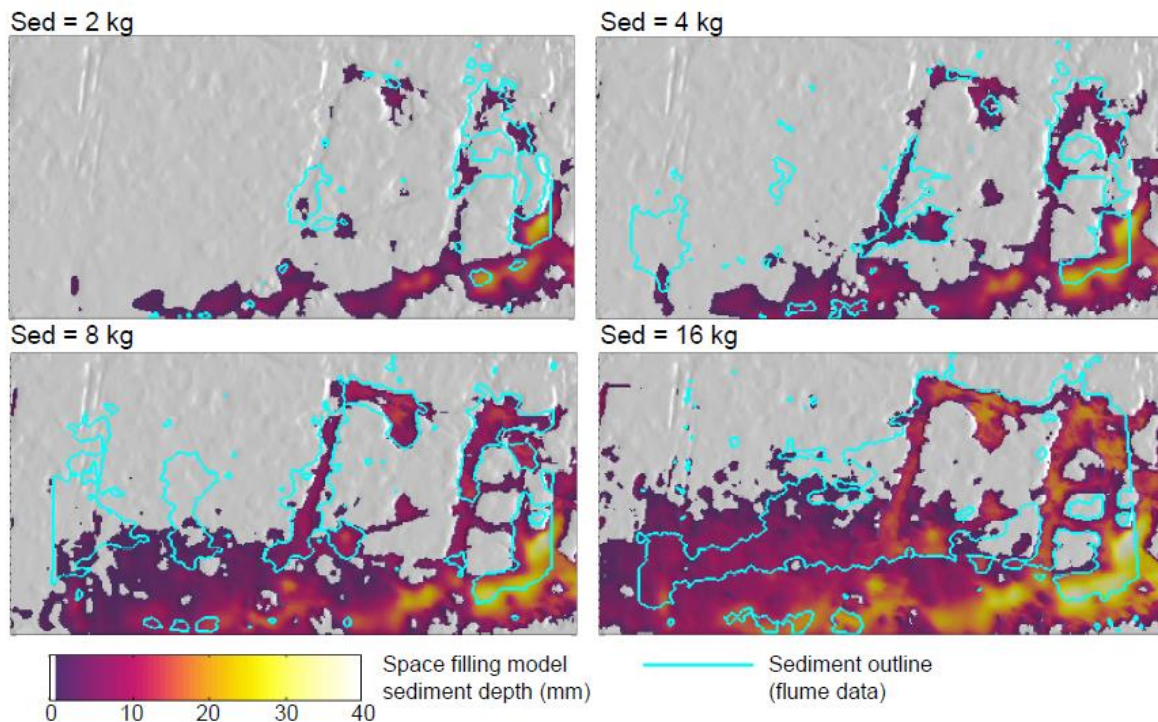
284



285
 286 *Figure 4: In each sub-plot, white bars show the distribution of either a) bed elevation or b) Δ_z*
 287 *across the entire bed. Δ_z is the difference between local and maximum upstream bed elevation*
 288 *over a 300 mm distance. Black bars show the distributions of these two properties for areas*
 289 *of the bed that had initial sediment cover in each run. The red line shows the mean elevation*
 290 *or Δ_z for all covered areas of the bed. Dashed cyan lines show the maximum elevation of the*
 291 *sediment cover produced by the same mass of sediment and a simple space filling model.*

292 Although some sediment is deposited at most elevations across the entire modelled reach, the
 293 majority of sediment is deposited on lower elevation areas of the bed. As the volume of
 294 sediment increases, in experiments with initial discharge of 20 and 35 l s⁻¹, the mean
 295 elevation of sediment covered areas increases from 31 to 39 mm (Q20/S2 to Q20/S16) and
 296 from 30 to 40 mm (Q35/S4 to Q35/S16) (Figure 4). Runs at 50 l s⁻¹, however, display the
 297 inverse pattern, with a drop in mean bed elevation as sediment mass increases from 2 to 8 kg;
 298 this pattern is related to the different locations of sediment deposition under a higher
 299 discharge (Figure 3). Bed elevation therefore seems to be an important, but not the only,
 300 control on sediment cover location.

301 Analysis of the hydraulic data in the companion paper shows that at $Q = 20 \text{ l s}^{-1}$, there was a
 302 negative correlation between downstream velocity and a topographic index, Δ_z . Δ_z is the
 303 difference between the local bed elevation and the maximum elevation over an upstream and
 304 lateral distance of 300 and $\pm 30 \text{ mm}$ respectively; these distances produced the highest
 305 correlations between topography and velocity [Hodge and Hoey, *in review*]. Relationships
 306 between velocity and bed elevation were not significant. Initial sediment cover in runs with Q
 307 = 20 and 35 l s⁻¹ is typically deposited in areas of the bed that are lower and have a higher Δ_z
 308 (Figure 4). As the sediment pulse mass increases, the cover extends to higher elevations and
 309 lower Δ_z . Consequently both elevation and Δ_z appear to influence the sediment location at
 310 initial discharges of 20 and 35 l s⁻¹.



311
 312 *Figure 5: Locations and depths of sediment patches predicted by a simple space filling*
 313 *model. Sediment outlines show location of initial sediment patches in experiments with $Q =$*
 314 *20 l s^{-1} and the same mass of sediment (Outlines are the same data as shown in Figure 3).*
 315 *Flow is from right to left. Bed area is 1.8 m long by 0.9 m wide. Experimental sediment*
 316 *patches are truncated within c.50mm of upstream and/or downstream ends because the*
 317 *photos did not cover the entire length of the test section*

318 The extent to which bed elevation determines the location of sediment patches is evaluated by
319 considering the spatial pattern of sediment cover that is produced by the space filling model.
320 The relationship between the input sediment mass and the depositional area predicted by the
321 space filling model is compared to experimental data in Figure 2. The model predicts a
322 curved relationship between sediment mass and area, with areas significantly greater than
323 observed in the experiments. For example, 4.5 kg of sediment in the space filling model
324 produces 23% sediment cover, whereas in flume run Q20/S8, 8 kg of sediment produces 20%
325 sediment cover. The larger model predictions occur in part because an unknown amount of
326 the sediment added in each run was transported out of the experimental section without being
327 deposited in a sediment patch. It would thus be appropriate to shift the entire space filling
328 model curve to the right in Figure 2, but the trapping efficiency of the bed, whether this
329 varies with input volume, and hence the magnitude of the shift, is unknown. Sediment
330 becomes more spread out in the flume experiments than in the space filling model as the
331 volume of sediment introduced increases (Figures 2 and 5). This slower lateral expansion in
332 the space filling model is confirmed by a power law fit to sediment cover predictions, which
333 has an exponent of 0.68 (± 0.029), indicating that as sediment mass increases, sediment area
334 increases at a slower rate in contrast to the linear fit to the flume data.

335 In addition to the differences in measured and predicted total cover, the space filling model is
336 also a poor predictor of the elevation and location of sediment patches (Figures 4 and 5). The
337 maximum elevation predicted by the space filling model is similar to the mean elevation of
338 the flume data (Figure 4), indicating that sediment is deposited at relatively higher elevations
339 in the flume. Furthermore, the single elevation predicted by the model omits all the variability
340 in the flume data. The space filling model correctly identifies some topographic depressions
341 where sediment collects, but it also over predicts the occurrence of patches along one side of
342 the flume (Figure 5). The elevation is relatively low along this side of the flume, but the flow
343 velocities are comparatively high (see Figure 3 and companion paper); consequently this is
344 not a site of sediment deposition in the experiments. Alternative variants on the space filling
345 model that also incorporated values of Δ_z did not produce better predictions of sediment patch
346 location.

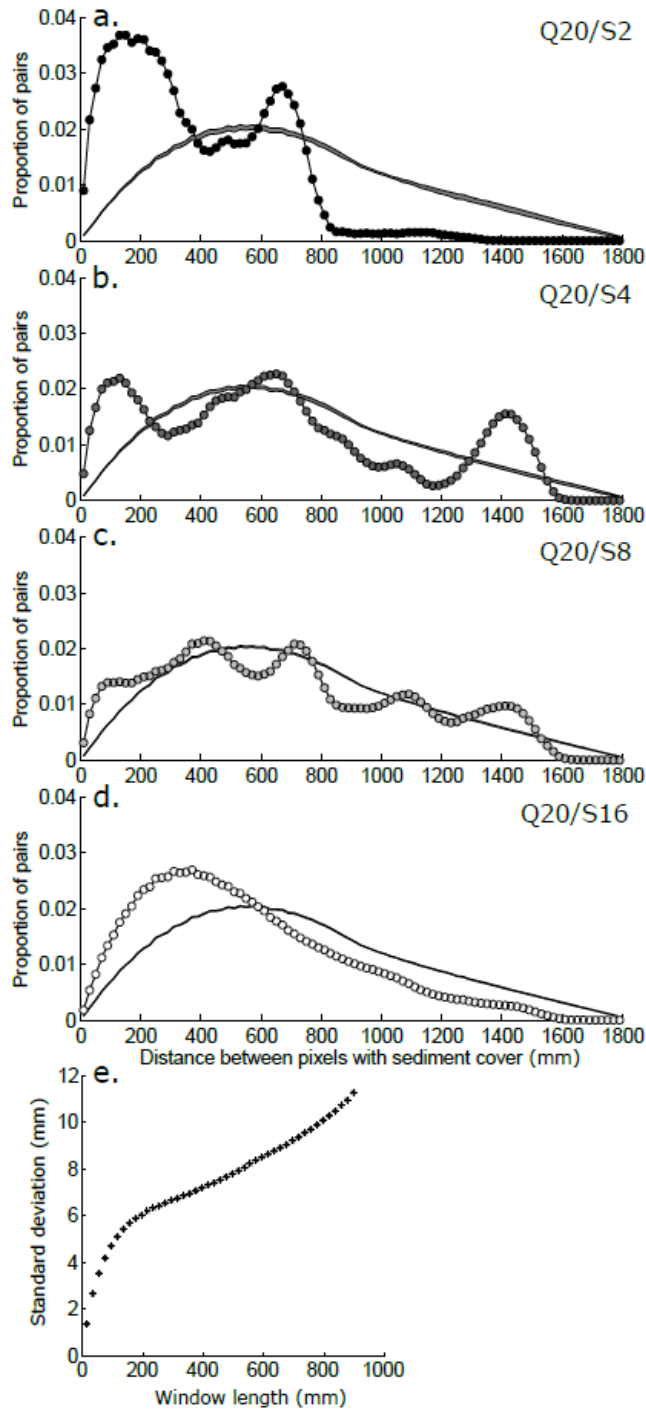
347 Using results from both the space filling model (Figures 2 and 5) and the measured
348 hydraulics (Figure 3), both bed elevation and Δ_z are important factors affecting sediment
349 patch location, but neither is sufficient to predict it. The spatial pattern of flow also needs to
350 be considered, noting that this will itself vary with sediment cover.

351 4.3. Length scale of initial sediment cover

352 The length scale of the initial sediment cover was analysed by calculating the distances
353 between all pairs of pixels that contained sediment; distributions of these distances are shown
354 in Figure 6 for runs Q20/S2 through Q20/S16. Results from a random distribution of
355 sediment cover are also shown for comparison; a random distribution would be expected in
356 the case that there was no influence of the topography (nor grain-grain interactions). In
357 Q20/S2, the modal distances are between 90 and 210 mm, with a secondary peak at 670 mm,
358 and the distribution is different from a random arrangement of grains. The primary and
359 secondary peaks likely correspond to distances between grains in the same patch, and in

360 different patches, respectively. These peaks are still present in Q20/S4, but the first peak is
361 smaller and there is an additional peak at 1430 mm. The first and last peaks show the biggest
362 difference from a random distribution. At Q20/S8 there are multiple peaks, although the
363 overall trend is not dissimilar to a random distribution. At Q20/S16 there is a smooth
364 distribution with a mode at 370 mm; the shape is similar to a random distribution, although
365 the mode is at a shorter length. These distributions demonstrate how, as sediment volume
366 increases, the sediment cover transitions from being clustered to being evenly distributed
367 across the entire bed.

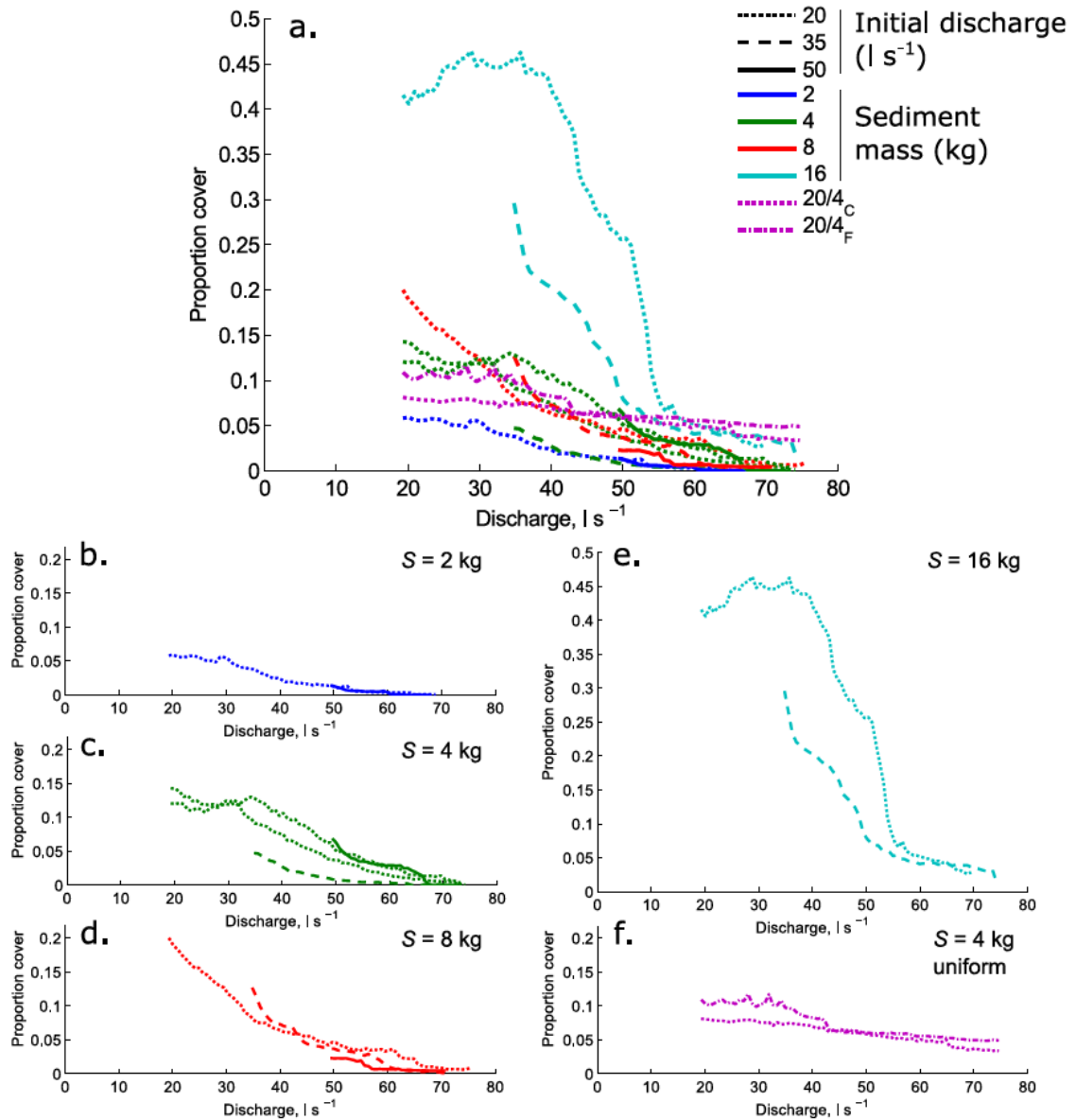
368 The spatial scales at which the sediment is clustered are similar to those identified in the
369 companion paper as being a characteristic length scale of the bedrock topography (150 mm,
370 Figure 6e). The topographic roughness of the flume bed varies as a function of the scale at
371 which it is measured. Roughness was defined as the standard deviation of bed elevations (σ_z)
372 [e.g. *Finnegan et al.*, 2007; *Johnson and Whipple*, 2007; *Inoue et al.*, 2014], and calculated
373 using a moving window. As window sizes increase up to about 150 mm, there is a rapid
374 increase in the mean value of σ_z (Figure 6e). At larger window sizes the mean continues to
375 increase, but at a slower rate. A semi-variogram analysis of bed elevations in the downstream
376 direction also reaches a sill value at about 150 mm. These results suggest that a window size
377 of 150 mm is the minimum required to capture the topographic complexity of the bed, and as
378 such may represent a horizontal length scale for the bedrock topography, and consequently
379 may also be linked to the dimensions of sediment patches.



380
 381 *Figure 6: a) to d) Distributions of the distances between each pixel that contains sediment*
 382 *and every other sediment containing pixel. Data are from runs Q20/2 through Q20/16. Grey*
 383 *bands show the 95% confidence interval calculated from spatially random distributions of the*
 384 *same numbers of grains. e) Mean of the standard deviation of elevations (σ_z) calculated from*
 385 *the bedrock topography, using moving windows of different lengths. The data in e) are taken*
 386 *from Figure 8 in the companion paper.*

387

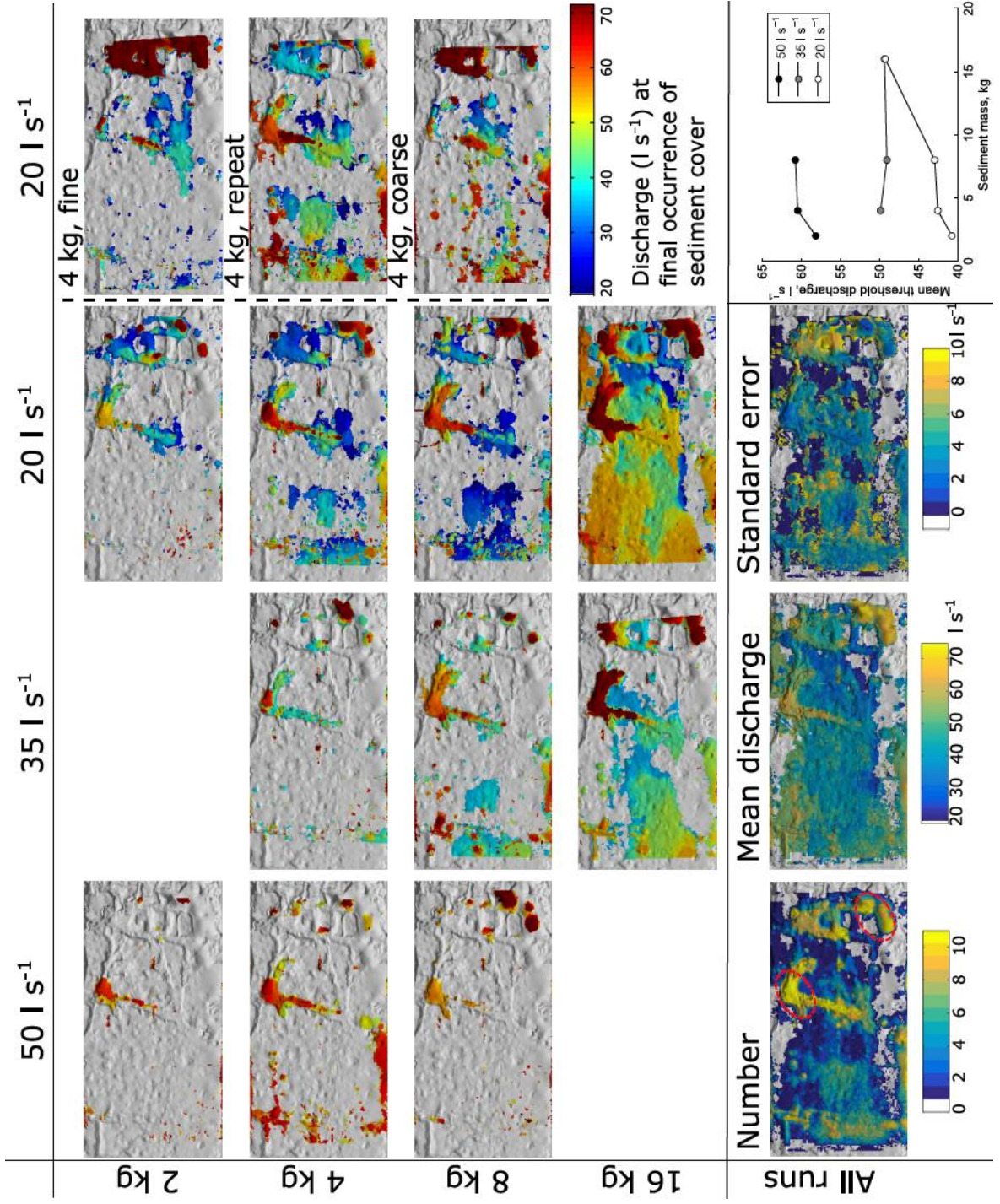
388 **4.4. Erosion of sediment cover**



390
 391 *Figure 7: a) Time series of total sediment cover from all experiments. b) to f) Subplots show*
 392 *the same data but separated out by sediment volume and grain size. The run conditions are*
 393 *indicated by the combination of colour (sediment mass) and line style (initial discharge).*
 394 *Sediment cover is normalised by the area of the flume that was visible in the photos. c) shows*
 395 *the consistency in behaviour of the two repeat runs with Q20/S4.*

396 Analysis of the formation of sediment cover has demonstrated the importance of both
 397 topography and flow in determining the location of sediment patches. After 5 minutes of
 398 steady flow in which sediment patches formed, the discharge was steadily increased to assess
 399 the patch stability. In most runs, sediment cover remained relatively constant until a
 400 discharge of between 30 and 35 l s⁻¹, at which point cover started to decrease as the patches
 401 began to be entrained (Figure 7a). Run Q20/S16 has an initial increase in sediment cover,
 402 because as sediment starts to be mobilised, it initially is more spread out over the bed before
 403 starting to be removed from the test section.

404 The patterns of decrease in sediment cover broadly fall into three regimes, depending on the
 405 mass of the sediment pulse. The first regime comprises runs with 2 kg pulses, with Q35/S4
 406 also showing the same trend. The second regime comprises all other 4 kg and the 8 kg runs,
 407 and the final regime comprises the 16 kg runs. The similarity between the 4 and 8 kg runs is
 408 in contrast to the differences in initial sediment cover between these runs. The excess
 409 sediment cover in the 8 kg runs is quickly eroded once the flow starts to increase, collapsing
 410 the erosion curve onto that of the 4 kg runs. The decreases in sediment cover are a mixture of
 411 gradual decreases and steps, suggesting grain-by-grain removal of sediment from around
 412 patch edges and rapid destabilisation of an entire sediment patch, respectively.



413

414 *Figure 8: Maps of discharge at which sediment is last present (threshold discharge, Q_t) at*
415 *each location across the flume bed. Grey indicates no sediment cover at that location during*
416 *that run. The sediment cover map includes all areas of the bed that contained sediment cover*
417 *at any point during the run, not just sediment cover after the initial 5 minutes. Flow is from*
418 *right to left. Bed area is 1.8 m long by 0.9 m wide. n. shows the number of runs with*
419 *sediment cover in each area of the bed, o. shows the mean flow to remove sediment cover and*
420 *p. shows the standard error of the mean. Data are from all experiments, including the two*
421 *runs with uniform sediment (k. and m.). In n., red ovals identify areas of persistent sediment*
422 *cover; the ‘elbow’ feature on the channel right, and the upstream pool on the left. The inset*
423 *graph in q. shows the mean threshold discharge for each run (i.e. the mean of all discharges*
424 *shown in panels a. to m.).*

425 Figures 8n to p compile spatial data of sediment cover from all 13 experiments; although the
426 experiments do have varying masses of sediment and initial discharges, the combined set
427 identifies the consistent features in the deposition and erosion of sediment cover. There is
428 persistence in sediment patch location between runs, with sediment patches most consistently
429 occurring in the low areas of the bed around the upstream blocks; in particular the ‘elbow’
430 feature and upstream pool (circled in red in Figure 8n). The stability of sediment cover within
431 these locations is also demonstrated by the high mean discharge at which these sediment
432 patches are eroded (Figure 8o). The standard error of the mean discharge in these locations is
433 relatively low (Figure 8p), indicating similarity between runs. Other areas of the bed display a
434 far higher standard error of the mean flow, hence greater variation between runs.

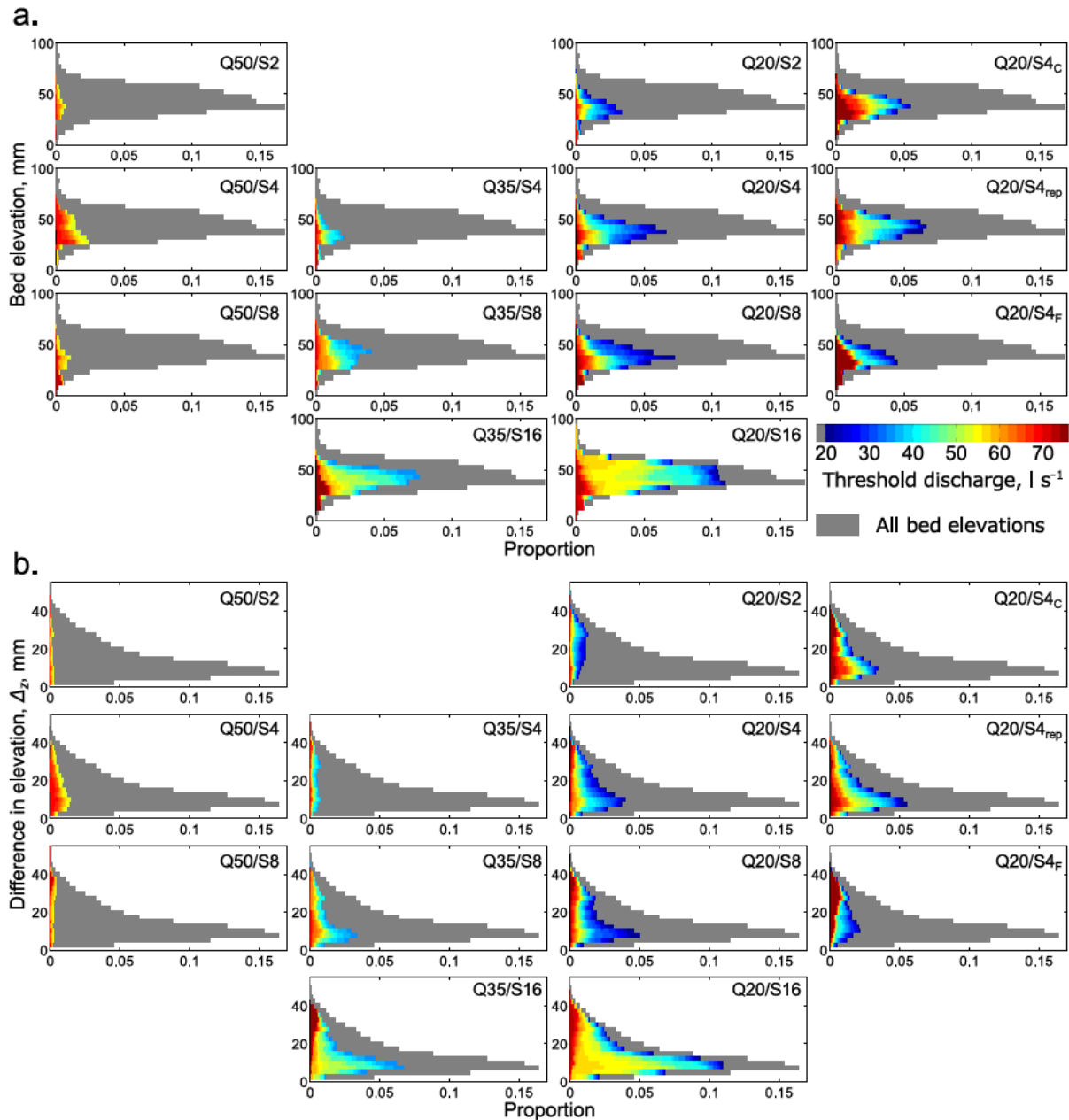
435 For each of the experimental runs, the discharge at which sediment cover in different
436 locations was eroded is shown in Figures 8a to m. These figures are produced by mapping the
437 maximum discharge at which each section of the bed surface was last covered with sediment
438 (termed the threshold discharge, Q_t). Consequently, the maps of Q_t give an indication of the
439 stability of sediment patches in different locations. Some sediment is re-deposited and
440 subsequently remobilised during the run, and so some sediment patches form during the
441 experiments as a result of upstream sediment entrainment. In these maps of Q_t the bed tends
442 to be segmented into distinct areas, with relatively abrupt transitions between areas with
443 different threshold discharges (Figures 8a to m). This indicates that areas of sediment patches
444 are removed in single erosional events; visual analysis of the experiment showed that this
445 process was often initiated by entrainment of one or two key grains, which destabilised the
446 surrounding patch. Such a process has also been observed for sediment patches on a flat bed
447 [Hodge *et al.*, 2016]. Patch shrinkage through grain-by-grain removal around the edge seems
448 to be less common, although the coloured fringes around some of the more stable patches and
449 across some of the widespread initial cover in Figures 8a to 8m indicate that it does occur.
450 The relatively gradual decrease in cover shown in Figure 7 therefore hides the fact that, at
451 any one time, sediment is sourced from distinct areas of the bed rather than from across the
452 entire bed.

453 For each run we calculate $\overline{Q_t}$, which is the mean of Q_t , (i.e. for Figures 8a through m, it is the
454 mean of all of the displayed discharges). $\overline{Q_t}$ for each run varies with sediment mass and initial

455 discharge (Figure 8q). There is an increase in \overline{Q}_t of $\sim 2 \text{ l s}^{-1}$ when sediment mass increases
456 from 2 to 4 kg. In contrast, values of \overline{Q}_t for 4 and for 8 kg of sediment are very similar to
457 each other, indicating that doubling the volume of sediment in the flume does not make the
458 sediment patches more stable. For the 20 l s^{-1} runs, increasing the sediment mass from 8 to 16
459 kg produces a further increase in \overline{Q}_t of 6 l s^{-1} , indicating that the sediment patches become
460 more stable. This increased stability is not seen in the 35 l s^{-1} runs.

461 Patches formed from uniform sediment are more stable than those in most of the mixed
462 sediment runs. All of the mixed sediment patches decreased in extent with increasing
463 discharge, but the uniform sediment patches show little erosion (Figure 7, and Figures 8k and
464 m). The uniform runs have the highest sediment cover at the end of the experiment, with only
465 the mixed 16 kg runs having similar levels of cover. The spatial pattern of Q_t (Figures 8k and
466 m) shows that sediment patches of uniform grains form in some of the same places as in the
467 mixed sediment runs, but that there are additional locations where uniform sediment patches
468 are more stable than mixed sediment patches. Both uniform sediments are comprised of
469 angular grains (0.2 on the Krumbein roundness scale; *Krumbein*, 1941), compared to the
470 typically sub-rounded sediments of the mixed sediment (0.5 on the Krumbein scale). The
471 results suggest that grain shape can affect grain-grain and grain-bed interactions and hence
472 patch stability.

473 **4.5. Topographic controls on the erosion of sediment cover**



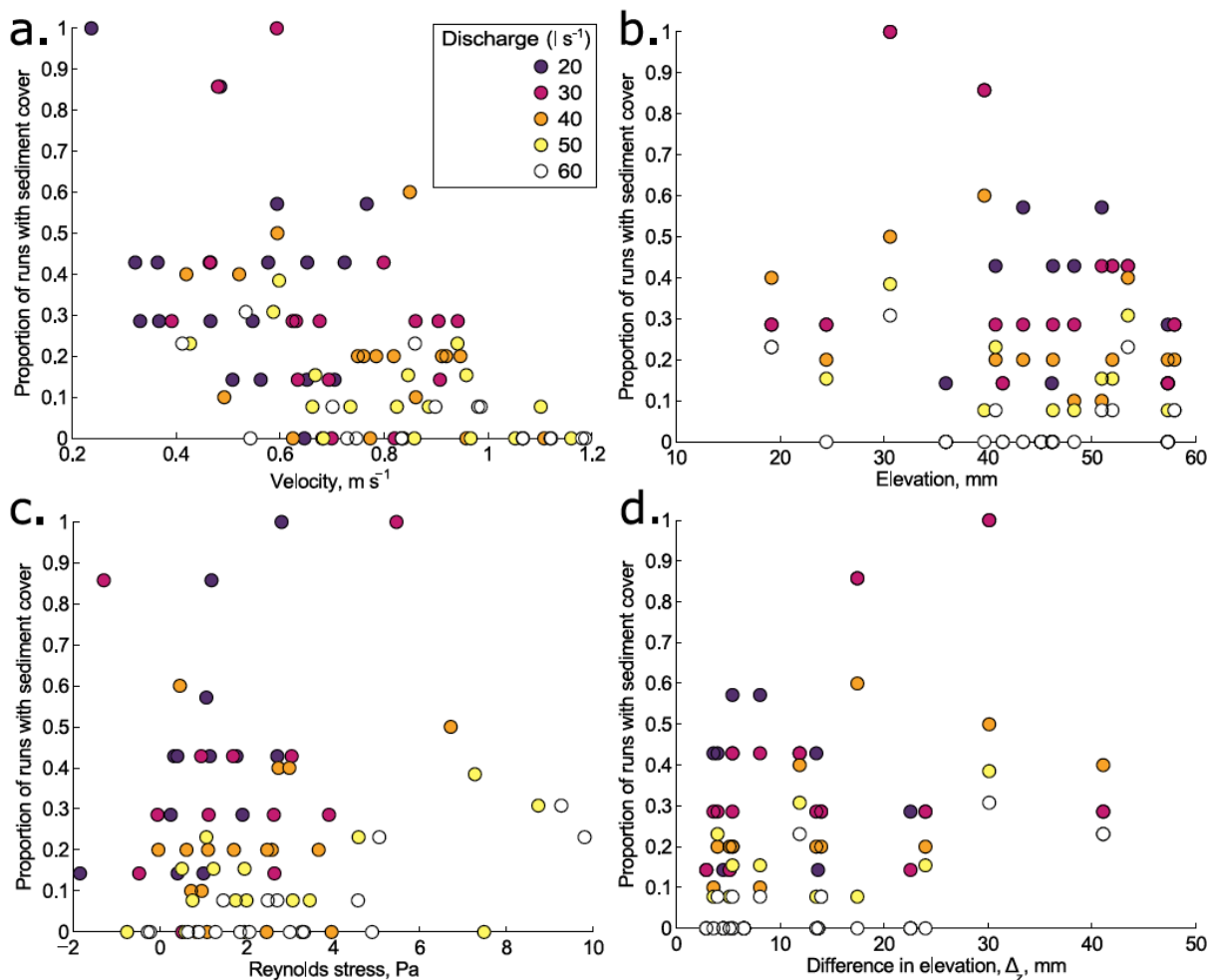
475
 476 *Figure 9: The threshold discharge (Q_t) at which sediment was eroded related to (a) bed*
 477 *elevation, and (b) Δ_z . Δ_z is the difference between local and maximum upstream bed elevation*
 478 *over a 300 mm distance. In each panel, grey bars show the distribution of either bed*
 479 *elevations or Δ_z . Coloured bars show the proportion of each elevation/ Δ_z that was covered in*
 480 *sediment during that experimental run, and the colours show the discharge at which that*
 481 *sediment was eroded (Q_t).*

482 Both bed elevation and Δ_z were found to influence the initial location of sediment cover
 483 (Figure 4); Figure 9 shows how both of these properties also influence values of Q_t . There is
 484 a general tendency for sediment stability to increase at lower elevations; however, both stable
 485 sediment and unstable sediment that is eroded first come from a wide range of elevations.
 486 Sediment is also more stable at higher values of Δ_z , with a more consistent pattern of
 487 increased stability than is shown for elevation.

488 The similarities between Q20/S4 and Q20/S8 again demonstrate that they have a similar
 489 regime, despite differences in their initial sediment cover. This similarity is because the extra
 490 sediment that is deposited in Q20/S8 is soon eroded. Run Q20/S16 shows relatively stable
 491 sediment cover in locations that have both a high elevation and low value of Δ_z , indicating
 492 that another factor (likely grain-grain interactions) is increasing its stability. The uniform
 493 sediment runs also show higher stability across a wider range of elevations and Δ_z than the
 494 mixed sediment runs, again suggesting that interactions between these angular grains are
 495 stabilising the sediment patches.

496 The discharge at which sediment is introduced is also important. The small amount of
 497 sediment that is deposited in runs Q50/S8 is only deposited in very stable areas of the bed.
 498 Sediment introduced at a lower discharge tends to be more stable at a higher discharge,
 499 whereas sediment that is put into the flume at that higher discharge is unable to form stable
 500 sediment patches. This may be because sediment that is already in the flume influences the
 501 local hydraulics and/or exhibits greater stability through grain-grain interactions;
 502 consequently the relative timing of sediment supply and flow events is also an important
 503 control on sediment stability.

504 **4.6. Relationships between sediment cover, flow velocity and bed topography**



505
 506 *Figure 10: Relationships between flow hydraulics (downstream velocity and Reynolds stress),*
 507 *topographic indices (elevation and Δ_z), and the occurrence of sediment cover at 18 locations*

508 across the flume. Hydraulic data are from experimental runs in the companion paper at 20,
 509 30, 40, 50 and 60 $l s^{-1}$ without sediment cover (as shown in Figure 3, right column), whereas
 510 the sediment cover data are from the sediment erosion components of the experiments
 511 presented here. The two datasets are therefore not strictly comparable, but the hydraulic data
 512 gives a useful indication of the likely conditions during the sediment runs. The 18 locations
 513 are shown in Figure 3. For the erosional component of each experimental run, we identify
 514 whether sediment cover was present at each of the 18 locations when Q was equal to each of
 515 the 5 discharges (20 though to 60 $l s^{-1}$). The proportion of runs is the number of occurrences
 516 of sediment cover over the number of times that those hydraulic conditions occurred.

517 The relative importance of topography and hydraulics can be ascertained through a
 518 comparison of the sediment erosion dataset with the hydraulic data collected in the runs
 519 without sediment cover [presented in Figure 3 and *Hodge and Hoey, in review*]. These two
 520 datasets are independent and therefore not strictly comparable as the hydraulic data do not
 521 include the changes in local roughness and velocity caused by the sediment cover [as
 522 demonstrated in *Hodge and Hoey, in review*]. However, on the assumption that the presence
 523 of sediment increases roughness and so will decrease velocities, the hydraulic data can be
 524 used as an upper estimate. Over all discharges, Figure 10a shows a significant negative
 525 relationship ($p < 0.001$) between downstream velocity and the proportion of runs with
 526 sediment cover. Δ_z and elevation produce significant positive ($p = 0.002$) and weakly
 527 significant negative ($p = 0.06$) relationships respectively (Figures 10b and d). Reynolds stress
 528 (Figure 10c), and σ_z (calculated using a 150 mm window) do not produce significant
 529 relationships. Using the data from all discharges, stepwise regression of the proportion of
 530 runs with sediment cover against the five hydraulic and topographic variables only retains
 531 velocity ($p < 0.001$), so velocity is the main control. Other variables are not included because
 532 of autocorrelation between variables.

533 Further analysis segmented the dataset by discharge, and regressed proportion of runs with
 534 sediment cover against each of the five variables (Table 1). Each of velocity, Δ_z and Reynolds
 535 stress produce significant relationships, primarily at higher discharges. The gradient of the
 536 relationships with velocity and Δ_z are as expected (negative and positive respectively; Table
 537 1). However, the relationships with Reynolds stress are positive (Table 1), which is counter to
 538 the idea that increased stress would inhibit sediment cover. This result may indicate the
 539 influence of a third factor which both increases turbulence and encourages sediment
 540 deposition. We therefore consider velocity and Δ_z to be the main controls on sediment cover
 541 development. One source of uncertainty in this analysis is the different input sediment
 542 masses; a lack of sediment cover could result from a lack of sediment supply instead of the
 543 hydraulic conditions. Therefore the occurrences of sediment cover are underestimates of what
 544 would happen with a continuous sediment supply.

	Discharge ($l s^{-1}$)				
	20	30	40	50	60
Velocity	-0.56	-0.63	-0.38	-0.34	-0.23
Reynolds stress	0.12	0.04	0.03	0.02	0.03
Elevation	-0.00	-0.01	-0.01	-0.00	-0.00

Δ_z	0.01	0.01	0.01	0.01	0.01
σ_z	-0.01	0.00	0.00	0.00	0.01

545 *Table 1: Gradients of linear regressions between the proportions of runs with sediment cover*
546 *and five different hydraulic and topographic variables. Relationships with $p < 0.05$ and $p <$*
547 *0.1 are indicated.*

548 **4.7. Sediment stability compared to flat-bed conditions**

549 In order to assess the impact of the bed topography on sediment stability, our data are
550 compared to results in *Hodge et al. [2016]*, which used the same uniform sediment as in runs
551 Q20/S4_C and Q20/S4_F, but on a flat, plywood, flume bed, onto which a layer of medium sand
552 grains was glued to add roughness. The flat-bed experiments took two forms: 1) individual,
553 isolated fine or coarse grains were placed in the centre of the flume and the discharge
554 increased until the grains were entrained; and 2) sediment was added to the flume in bulk
555 under steady flow conditions, forming a combination of sediment patches and isolated grains.
556 Discharge was increased until the isolated grains and patches were entrained.

557 Individual fine and coarse grains on this flat-bed moved at respective discharges of 6 and 8 l
558 s⁻¹. When a pulse of sediment was added to the flume and allowed to form patches, the
559 thresholds for initial sediment entrainment from the patches increased to 11 and 10 l s⁻¹ for
560 fine and coarse sediment, respectively. Across all experiments with sediment patches the
561 mean discharge at which grains were entrained from a patch was between 15 and 25 l s⁻¹. In
562 contrast, in the experiments with the 3D printed bed, patches of sediment were present in the
563 flume even at an initial discharge of 50 l s⁻¹. The mean threshold discharge for the erosion of
564 the sediment patches (\overline{Q}_t) was between 40 and 60 l s⁻¹. Furthermore, in the runs with uniform
565 coarse or fine sediment (as used in the flat bed experiments), sediment patches were still
566 stable in the flume at a discharge of 75 l s⁻¹. This stability demonstrates the importance of
567 bedrock morphology for maintaining sediment cover.

568 **5. Discussion**

569 The discussion addresses each of the research questions in turn, before considering the
570 broader implications for bedrock-alluvial channels and bedrock erosion.

571 **5.1. How does the amount of sediment cover vary with flow discharge and supplied** 572 **sediment mass?**

573 The initial sediment cover that forms on the bare bedrock bed after the first five minutes is a
574 linear function of the mass of sediment input to the flume (Figure 2). The relationships
575 between sediment mass and cover for the experiments with different initial discharges have
576 similar gradients, but are vertically offset from each other, such that the same sediment mass
577 produces less cover at a higher discharge. Consequently both sediment mass and initial
578 discharge significantly affect the sediment cover. The linear form of these relationships is
579 similar to those previously proposed from theoretical [*Sklar and Dietrich, 2004*] and flume
580 [*Chatanantavet and Parker, 2008*] analyses. These published relationships used a relative
581 sediment flux (defined as sediment supply over capacity sediment flux) whereas we use a
582 known mass of sediment. Figure 2 could be converted to a flux format by estimating a
583 capacity sediment flux, and normalising the sediment mass by the time it took to feed into the

584 flume. Such a calculation is likely to collapse the different relationships in Figure 2 onto each
585 other, but is not undertaken because of the uncertainties around estimating a capacity bedload
586 flux in a bedrock-alluvial channel.

587 One implication of the use of a single pulse, rather than a constant flux, of sediment is that
588 the experiments represent a dynamic, rather than an equilibrium, condition. At low sediment
589 inputs in these experiments, sediment cover may be under-developed compared to what
590 would be produced by even a small, constant flux. In these experiments it is possible to have
591 areas where sediment patches would be stable were they to develop, but which were
592 overpassed by the input sediment. With a longer duration sediment feed there would be a
593 greater chance of these areas developing sediment cover. Constant feed conditions may mean
594 that there is less difference in sediment cover between the different sediment inputs than is
595 observed in these experiments, which may further enhance the importance of the bed
596 topography. However, sediment inputs to many bedrock-alluvial channels in upland areas are
597 likely to be episodic and may or may not coincide with high flow events, so our experimental
598 conditions could be considered to be a more realistic starting point than would be a constant
599 sediment feed rate.

600 **5.2. To what extent does bed topography control sediment patch location?**

601 Comparison between the locations of initial sediment cover (Figure 4) indicates that sediment
602 is generally, but not exclusively, deposited in areas of the bed that are lower and have a
603 higher Δ_z . As the sediment pulse mass increases, the cover extends to higher elevations and
604 lower Δ_z (Figure 4). The exception to these trends is the 50 l s^{-1} runs. This could be because
605 of changes in local velocity making these areas no longer suitable for sediment deposition,
606 which is supported by the locations for which there is velocity data (seen in Figure 3).
607 Another explanation is that the higher flow velocities mean that the input sediment travels
608 further downstream before it reaches the bed, and thus overpasses the deepest areas in the
609 upstream section of the bed. The 50 l s^{-1} results may therefore be more influenced by the
610 experimental boundary conditions than the other runs. Analysis of the length scales of the
611 initial sediment cover shows clustering at small scales at Q20/S2 (Figure 6a), with
612 progressively less clustering at these scales as the amount of sediment cover increases and the
613 distributions become more similar to a random placement of sediment (Figures 6b to d). The
614 length scale of the initial clustering is similar to the minimum length scale needed to describe
615 the bed roughness. This identified length scale of 150 mm is likely to reflect the minimum
616 lateral dimension of bed hollows because: 1) the bed hollow dimension will constrain the
617 maximum distance between grains in the same sediment patch, and 2) in order for σ_z to reach
618 its maximum, the sample window will need to be large enough to include both the base of the
619 hollow and the surrounding high areas. The length scale analysis suggests that at low
620 sediment cover the bed topography is an important control on the spatial distribution of
621 sediment patches. As sediment cover increases, the length scale of the sediment patches
622 become independent of the channel topography.

623 **5.3. To what extent does bed topography control sediment patch stability?**

624 The bed topography has been demonstrated to influence the initial location of sediment
625 patches. The latter parts of the experiments with increasing discharge show that this

626 topography is also important for determining sediment patch stability. Furthermore, flat-bed
627 experiments with comparable sediment [Hodge *et al.*, 2016] show that without bed
628 topography sediment patches are entrained at far lower discharges. Analysis of the erosion of
629 sediment patches (Figure 7) identified three different regimes; within each regime the
630 experiment showed a similar decrease in sediment cover with increasing discharge, regardless
631 of the discharge at which the experiment was initiated. However, there are still differences
632 between runs within the same regime, indicating that there is also stochasticity in the
633 entrainment process.

634 The first regime comprised all runs with 2 kg of sediment and run Q35/S4; these runs had the
635 least sediment cover at any discharge (Figure 7a). In these experiments there was not enough
636 sediment to fill all the areas that could hold stable sediment patches at a given discharge.
637 Patch development was therefore supply-limited. The length scales of these sediment patches
638 were controlled by the bed topography (Figure 6a).

639 The 4 kg and 8 kg runs together comprised the second regime, with relatively small
640 differences between the amount of cover during the erosional phase despite the differences in
641 sediment input which led to some differences in initial cover that are quickly eradicated once
642 erosion starts (Figure 7a). The similarities suggest that, at any discharge, all potentially stable
643 areas of the bed are filled with sediment, and that any excess sediment (particularly in the
644 case of the 8 kg runs) is removed. The interaction between the bed topography and the flow
645 thus provides a template for sediment patch stability. Under this second regime, patch extent
646 is therefore a function of the interaction between the bed and the flow, rather than the amount
647 of sediment supplied.

648 The final regime is the 16 kg runs, which have disproportionately greater sediment cover
649 during the latter parts of the experiment (Figure 7a). In these runs the large volume of
650 sediment appears to override the influence of the bed topography, with no apparent
651 relationship between the length scales of the sediment patches and the topography (Figure 6).
652 The patches are more extensive and more stable than would be predicted from earlier runs; if
653 topography was the only factor influencing the stability of sediment patches that formed in
654 these areas, then it seems likely that sediment cover would also have formed in runs with less
655 sediment. The increased stability of the sediment patches could be because of grain-grain
656 interactions increasing the critical shear stress for grain entrainment, e.g. through sheltering
657 effects and increased pivoting angles [Hodge *et al.*, 2011]. The same increase could be due to
658 the presence of sediment locally increasing the bed roughness, and hence decreasing the
659 ability of the flow to entrain the sediment [e.g. Johnson 2014; Inoue *et al.*, 2014]; such an
660 impact of sediment cover on flow was observed by Hodge and Hoey [*in review*]. The idea of
661 grain-grain interactions stabilising sediment cover is also supported by the observation that
662 this stable cover occurred on higher areas of the bed with lower values of Δ_z (Figure 10),
663 where the higher flow velocities [Hodge and Hoey, *in review*] might instead be expected to
664 make the sediment patches less stable, rather than the observed increase in stability.

665 Over these three regimes, the extent of sediment cover changes from being a function of
666 sediment supply when sediment is under-supplied, to a function of the interaction between

667 the bed and the flow, and then back to being a function of sediment supply again. On the
668 whole, the volume of the initial sediment input appears to be more important than the
669 discharge at which it is introduced. The only exception is that at high initial discharges
670 sediment may have too much momentum to be deposited in stable locations. Within each
671 regime there also appears to be fairly little memory in the system, with the sediment cover
672 quickly adjusting to the current flow conditions. This is demonstrated by the similarities
673 between the sediment cover erosion curves in Figure 7, which show a similar pattern for runs
674 with the same sediment mass but different initial discharges.

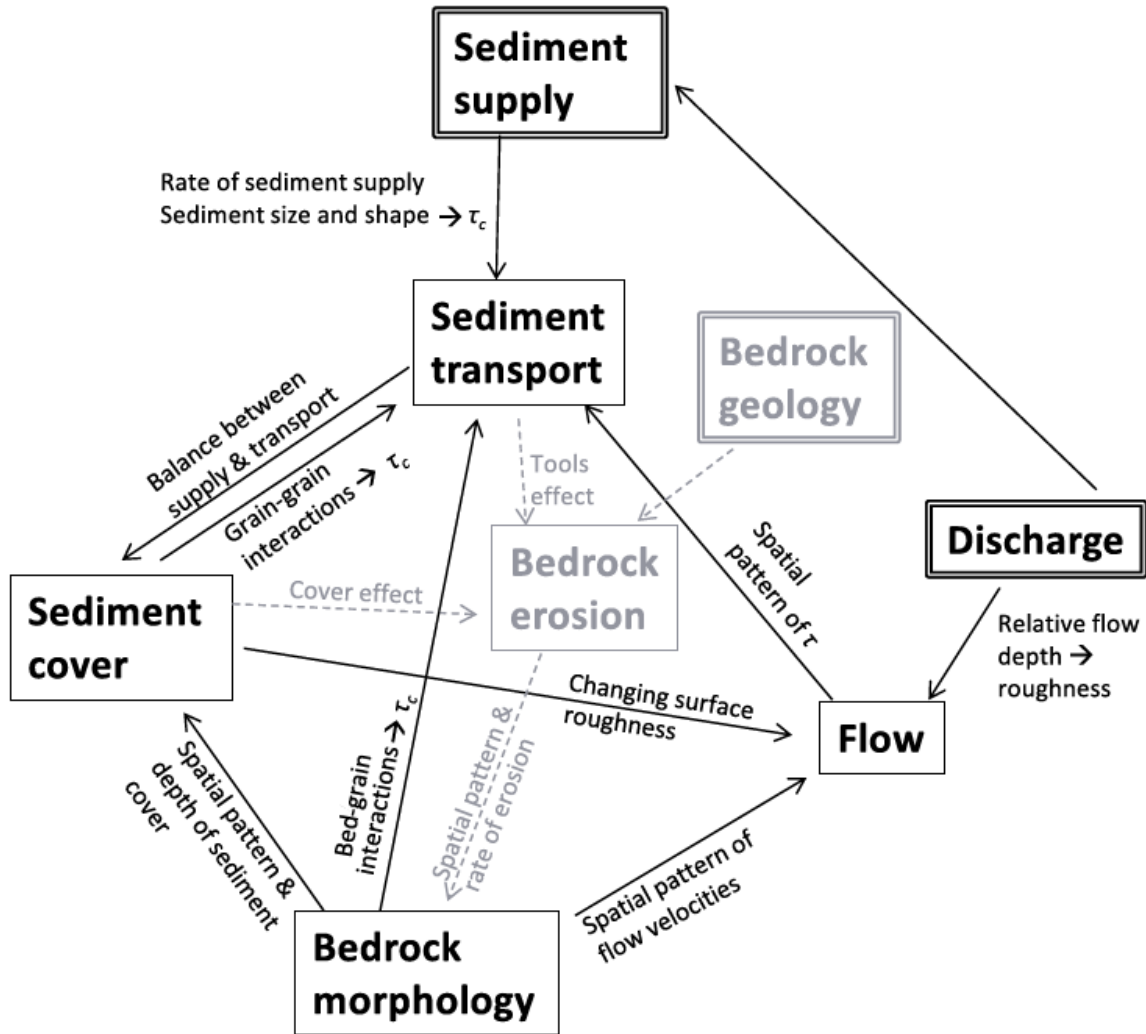
675 **5.4. What are the relationships between sediment patch occurrence, hydraulics and** 676 **local bed topography?**

677 Analysis of the locations where sediment patches formed, and their stability as they eroded,
678 demonstrated that both bed elevation and Δ_z are important, but not exclusive, controls. The
679 absence of spatially distributed hydraulic data meant that the only possible comparison was
680 with hydraulic data from runs without sediment cover (which neglects the influence that
681 sediment cover has on local velocity). This comparison showed that across all discharges,
682 velocity had the the most significant control on the occurrence of sediment cover (Figure 10).
683 At some individual discharges (Table 1), Δ_z and Reynolds stress also had a significant
684 relationship with the occurrence of sediment cover, although the relationship with Reynolds
685 stress was positive rather than negative as expected. These findings to an extent appear to
686 contradict previous studies, in which elevation has been identified as a controlling factor
687 [Johnson and Whipple, 2007; Turowski et al., 2008]. The filling model shows that in this case
688 infilling the bed produces poor predictions of both the mean elevation and the location of
689 sediment cover (Figure 4), so predictions of sediment cover location need to consider spatial
690 variation in flow velocity.

691 **5.5. Implications for bedrock-alluvial channels**

692 The flume experiments reported in this, and the companion, paper have demonstrated that
693 underlying bedrock topography has significant impacts on the hydraulic and sediment
694 transport processes and relationships that occur within a bedrock-alluvial channel. These
695 processes and relationships are outlined in Figure 11, which is an extension of alluvial
696 channel interaction models [e.g. Ferguson and Ashworth, 1986] to bedrock-alluvial systems.
697 Over short timescales and in these experiments, the bedrock morphology can be considered to
698 be fixed. However, over longer timescales and/or extreme events, the bedrock morphology
699 itself is an additional degree of freedom [Tinkler and Wohl, 1998].

700 This and the companion paper have quantified many of the relationships in Figure 11 through
701 demonstrating how a particular bedrock morphology controls sediment patch dynamics by: 1)
702 inducing a spatial pattern of flow velocities, and consequently 2) providing a template of
703 areas with greater or lesser sediment stability, as well as 3) controlling the relationship
704 between supplied sediment mass and patch area. Each of these relationships changes with
705 discharge. However, the degree to which the form of these relationships is specific to this
706 particular bed remains unknown. The particular combination in the prototype site of
707 relatively rough and smooth upstream and downstream areas, respectively, may maximise the
708 spatial variation in processes compared to other bed morphologies.



709
 710 *Figure 11: An adaptation of alluvial river process-form interaction models to bedrock-*
 711 *alluvial channels [e.g. Ashworth and Ferguson, 1986]. Black arrows indicate interactions*
 712 *over short timescales, grey arrows indicate interactions over timescales at which bedrock*
 713 *incision operates. Boxes with a double outline indicate an external control. This diagram*
 714 *assumes that bedrock incision is caused by sediment transport. Each arrow is labelled with a*
 715 *summary of the processes and factors causing the indicated interaction; processes in black*
 716 *have been addressed in this and the companion paper. τ and τ_c are shear stress and critical*
 717 *shear stress.*

718 The question of how to quantify bedrock morphology in a way that represents its influences
 719 on the processes in Figure 11 is unresolved, despite its clear importance in these processes
 720 [Chatanantavet and Parker, 2007; Finnegan et al., 2007; Johnson and Whipple 2007; Inoue
 721 et al., 2014]. Use of a single roughness length [e.g. Inoue et al., 2014; Johnson, 2014] is
 722 problematic because it varies with the window size over which it is measured (Figure 6e), and
 723 is non-directional. Furthermore, a single length scale does not account for the spatial
 724 variation in topography that controls the spatial extent of sediment patches under low and
 725 medium sediment supplies. We have demonstrated that one possible approach is to identify
 726 the minimum window size that is needed to capture the bed roughness (defined as σ_z), giving
 727 two length scales; a vertical standard deviation of elevations (σ_z), and an additional horizontal

728 length scale (i.e. the minimum window size). In these data, the latter length scale seems to be
729 linked to the size of sediment patches under low supply conditions.

730 The issue of identifying appropriate roughness scales is hampered by the lack of data on
731 sediment cover and topography from bedrock-alluvial channels. A systematic analysis of
732 such data may allow identification of an appropriate scale at which to measure roughness in
733 order to relate it to sediment patch properties. These data could also help to identify the key
734 factors that control channel roughness e.g. bedrock properties, abrasion processes or sediment
735 cover [Lamb *et al.*, 2015], but would also need to account for temporal variations in sediment
736 cover [e.g. Johnson *et al.*, 2009]. Sediment patches in bedrock-alluvial systems are equivalent
737 to bedforms in alluvial channels, and have been observed in some cases to have similar forms
738 [e.g. Hersen, 2005; Nittrouer *et al.*, 2011], and similarly can be considered to be either forced
739 (*i.e.* occupying topographic niches) or free (*i.e.* forming on areas of pseudo-plane bed
740 conditions). Nelson and Seminara [2012] demonstrate analytically how bedforms develop on
741 a flat bedrock bed, with results comparable to those observed by Chatanavet and Parker
742 [2008], but they do not extend the analysis to beds with a more variable topography, such as
743 in these experiments. Systematic field data would hence enable a classification of bedforms
744 in bedrock-alluvial systems to be developed, such as exists for gravel-bed channels [e.g.
745 Montgomery and Buffington, 1997], erosional features in bedrock [Richardson and Carling,
746 2005] and bedrock channel morphology [Wohl and Merritt, 2001]. Quantifying bedrock
747 morphology will again be necessary, because results presented here indicate that bedforms
748 will be driven by the bed topography at low sediment supplies, and become more similar to
749 alluvial ones at higher sediment fluxes.

750 Another question that remains to be fully addressed is to identify the conditions under which
751 within-reach variations are an important control on the processes in Figure 11 [Lague, 2014].
752 The companion paper [Hodge and Hoey, *in review*] demonstrated that even under high flow
753 conditions, there is considerable spatial variation in flow velocity and Reynolds shear stress,
754 with a reach-averaged approach likely to underestimate the magnitude of forces applied to the
755 bed and sediment [Ferguson, 2003]. The analysis of sediment cover shows that topographic
756 variation decreases in importance as the amount of sediment in the reach increases. Bed
757 topography will therefore also affect sediment transport at low and intermediate sediment
758 cover, as it will determine the locations of the sediment patches that the sediment grains
759 move between, in the same way that grain movement is controlled by pool-bar spacing in an
760 alluvial channel [Pryce and Ashmore, 2003].

761 The finding that large amounts of sediment can override other factors in the channel is
762 consistent with previous numerical modelling results [Lague, 2010; Hodge, 2015], and field
763 data from both bedrock-alluvial and alluvial rivers [e.g. Cui *et al.*, 2003; Turowski *et al.*,
764 2012]. Both Lague's [2010] and Hodge's [2015] models reproduced the development of
765 sediment cover under fluctuating sediment inputs, and found that significant sediment cover
766 was produced by occasional large (greater than channel capacity) sediment inputs, which
767 overrode the relationship that was otherwise produced between sediment flux and cover. The
768 flume results presented here demonstrate that similar effects can also occur on a more local
769 basis within the bed. This occurred when areas of extensive sediment cover demonstrated

770 enhanced stability relative to that which would be expected from runs with smaller sediment
771 inputs. None of these runs had complete sediment cover though, indicating that sediment
772 storage and enhanced stability does not only occur when the bed is fully alluvial. These
773 findings have similarity to the relationships between sediment volume and sediment transport
774 derived by *Lisle and Church* [2002] for degrading alluvial rivers. Differences between the
775 flume and model results reflects the importance of interactions between the topography, flow
776 and sediment transport that are not fully reproduced in either of the previous models.

777 **5.6. Implications for bedrock erosion**

778 A relationship between sediment flux and sediment cover is necessary for many models of
779 channel incision. The analysis of the initial sediment cover produced in the flume runs
780 supports the use of a linear relationship, as is already widely used [e.g. *Sklar and Dietrich*,
781 2004]. However, as already outlined, the single sediment input is not directly equivalent to a
782 constant flux. Furthermore, the analysis of the erosion of the patches and the identification of
783 three different regimes suggests that the relationship may be more complicated and may
784 depend on the magnitudes of flow events and the nature of sediment supply into the reach
785 (*i.e.* pulsed or continuous; timing relative to flow events). The similarity between the results
786 from the 4 kg and 8 kg runs suggests that under intermediate sediment inputs, sediment cover
787 may actually be insensitive to the exact value. Instead, the bed topography plays an important
788 role in determining the extent of sediment cover that is stable at a given discharge. There is
789 therefore a need to work out how the impact of this sub-reach heterogeneity can be upscaled
790 for calculations of long-term bedrock incision [*Lague*, 2014]. Such a development will
791 complement advances in understanding how inter-granular interactions affect the flux-cover
792 relationship [*Hodge and Hoey*, 2012].

793 This insensitivity of sediment cover to sediment input is consistent with the theoretical
794 predictions of cover fraction developed by *Inoue et al.* [2014]; they predict that with a
795 topographically rough bed, there is a relatively small change in sediment cover as relative
796 sediment flux increases from just over zero to equal to capacity. In contrast, with a smooth
797 bed, they predict no sediment cover at low fluxes, and a rapid increase at higher fluxes.
798 However, *Inoue et al.*'s [2014] relationship for rough beds only applies when the ratio of bed
799 roughness length (e.g. standard deviation of bed elevations) to grain size is 20. In the flume
800 experiments presented here, the ratio has a value of about 2 (σ_z for the entire bed is 12 mm,
801 and D_{50} is 7.3 mm). At a ratio of 2.5 *Inoue et al.* [2014] predict that no sediment cover should
802 form. This again highlights the importance of spatial variability in topographic roughness and
803 the need to address how the roughness and topography of bedrock-alluvial rivers are
804 quantified.

805 One component of Figure 11 that has not been addressed directly is the processes relating to
806 bedrock erosion. However, sediment cover controls the areas of the bed that can be eroded. It
807 has been observed in the field, flume and numerical experiments [*Finnegan et al.*, 2007;
808 *Johnson and Whipple*, 2007; *Turowski et al.*, 2008; *Nelson and Seminara*, 2011] that
809 sediment cover collects in the lowest parts of the bed, meaning that erosion is focussed at
810 higher elevations, potentially widening the channel [*Turowski et al.*, 2008; *Yanites and*
811 *Tucker*, 2010; *Nelson and Seminara*, 2011]. However, sediment does not exclusively collect

812 at low elevations in these experiments (Figure 5), indicating that the pattern of flow may be
813 an important control on the spatial pattern of erosion and hence the morphological evolution
814 of the channel.

815 **6. Conclusion**

816 A 1:10 scale Froude model of a bedrock-alluvial channel was used to measure sediment
817 dynamics on a scaled prototype channel morphology. Our findings are that: 1) sediment
818 patches tend to initiate in the lowest areas of the bed, but areas of high flow velocity can
819 inhibit this; 2) at low sediment inputs the extent of sediment patches is determined by the bed
820 topography and can be insensitive to the exact volume of sediment supplied; and 3) at higher
821 sediment inputs more extensive patches are likely stabilised by grain-grain and grain-flow
822 interactions, and there is a lesser influence of the bed topography. These results imply that the
823 bed topography, hydraulics and grain-grain interactions can all be strong influences on the
824 spatial pattern and stability of sediment patches, and hence the areas of the bed that are
825 protected from erosion and the pathways of bedload transport. The non-linear interactions
826 between topography, hydraulics and sediment processes mean that the resulting patterns of
827 hydraulics and sediment cover cannot be easily upscaled to a reach-average value. There is
828 therefore a need to develop metrics of channel morphology that account for its spatial
829 influence on hydraulics and sediment processes. The range of initial discharges and sediment
830 input masses used here simulates a range of scales of sediment supply events, and a range of
831 ratios of sediment supply to discharge (transport capacity). These results provide further
832 evidence for the significance of the timing and magnitude of sediment supply and flow events
833 in upland rivers.

834 **7. Acknowledgements**

835 This project was supported by the Royal Geographical Society (with IBG) with a Small
836 Research Grant awarded to RAH. Thanks to Kenny Roberts and Tim Montgomery for
837 laboratory assistance. We thank the Editor, AE, Peter Nelson and two anonymous reviewers
838 for their thorough reviews and useful suggestions. Data are available from the corresponding
839 author by request.

840 **References**

- 841 Ashworth, P.J. and R. I. Ferguson (1986). Interrelationships of channel processes, changes
842 and sediments in a proglacial braided river, *Geogr Ann A.*, 68, 361-371.
- 843 Chatanantavet, P., and G. Parker (2008), Experimental study of bedrock channel alluviation
844 under varied sediment supply and hydraulic conditions, *Water Resour. Res.*, 44(12),
845 doi:10.1029/2007WR006581.
- 846 Cui, Y., G. Parker, T. E. Lisle, J. Gott, M. E. Hansler-Ball, J. E. Pizzuto, N. E. Allmendinger,
847 and J. M. Reed (2003), Sediment pulses in mountain rivers: 1. Experiments, *Water Resour.*
848 *Res.*, 39(9), 1239, doi:10.1029/2002WR001803.
- 849 Ferguson, R. I. (2003), The missing dimension: effects of lateral variation on 1-D
850 calculations of fluvial bedload transport, *Geomorphology*, 56(1–2), 1–14,
851 doi:10.1016/S0169-555X(03)00042-4.

852 Finnegan, N. J., L. S. Sklar, and T. K. Fuller (2007), Interplay of sediment supply, river
853 incision, and channel morphology revealed by the transient evolution of an experimental
854 bedrock channel, *J. Geophys. Res.*, 112(F3), doi:10.1029/2006JF000569.

855 Goode, J. R., and E. Wohl (2010), Coarse sediment transport in a bedrock channel with
856 complex bed topography, *Water Resour. Res.*, 46, W11532, doi:10.1029/2009WR008135.

857 Hersen, P. (2005), Flow effects on the morphology and dynamics of aeolian and subaqueous
858 barchan dunes, *J. Geophys. Res.*, 110(F4), F04S07, doi:10.1029/2004JF000185.

859 Hodge, R.A. (2015), Sediment processes in bedrock-alluvial rivers: Research since 2010 and
860 modelling the impact of fluctuating sediment supply on sediment cover, presented at Gravel
861 Bed Rivers 8: Gravel Bed Rivers and Disasters, Kyoto and Takayama, Japan, 14-18 Sept.
862 <https://www.youtube.com/watch?v=IDHBvasrAKY>

863 Hodge, R. A., and T. B. Hoey (2012), Upscaling from grain-scale processes to alluviation in
864 bedrock channels using a cellular automaton model, *J. Geophys. Res. Earth Surf*, 117,
865 F01017, doi:10.1029/2011JF002145.

866 Hodge, R. A., T. B. Hoey, and L. S. Sklar (2011), Bedload transport in bedrock rivers: the
867 role of sediment cover in grain entrainment, translation and deposition, *J. Geophys. Res.*,
868 doi:10.1029/2011JF002032.

869 Hodge, R., T. Hoey, G. Maniatis, and E. Leprêtre (2016), Formation and erosion of sediment
870 cover in an experimental bedrock-alluvial channel, *Earth Surf. Process. Landforms*,
871 doi:10.1002/esp.3924.

872 Huda, S. A., and E. E. Small (2014), Modeling the effects of bed topography on fluvial
873 bedrock erosion by saltating bed load, *J. Geophys. Res. Earth Surf*, 119(6), 1222–1239,
874 doi:10.1002/2013JF002872.

875 Inoue, T., N. Izumi, Y. Shimizu, and G. Parker (2014), Interaction among alluvial cover, bed
876 roughness and incision rate in purely bedrock and alluvial-bedrock channel, *J. Geophys. Res.*
877 *Earth Surf.*, 2014JF003133, doi:10.1002/2014JF003133.

878 Johnson, J. P. L. (2014), A surface roughness model for predicting alluvial cover and bed
879 load transport rate in bedrock channels, *J. Geophys. Res. Earth Surf*, 2013JF003000,
880 doi:10.1002/2013JF003000.

881 Johnson, J. P. L., and K. X. Whipple (2010), Evaluating the controls of shear stress, sediment
882 supply, alluvial cover, and channel morphology on experimental bedrock incision rate, *J.*
883 *Geophys. Res.*, 115, F02018, doi:10.1029/2009JF001335.

884 Johnson, J. P. L., K. X. Whipple, L. S. Sklar, and T. C. Hanks (2009), Transport slopes,
885 sediment cover, and bedrock channel incision in the Henry Mountains, Utah, *J. Geophys.*
886 *Res.*, 114(F2), doi:10.1029/2007JF000862.

887 Johnson, J. P., and K. X. Whipple (2007), Feedbacks between erosion and sediment transport
888 in experimental bedrock channels, *Earth. Surf. Process. Landforms*, 32(7), 1048–1062,
889 doi:10.1002/esp.1471.

890 Krumbein, W. C. (1941) Measurement and geological significance of shape and roundness of
891 sedimentary particles. *J. Sedimentary Research* 11 (2), 64-72.

892 Lague, D. (2010), Reduction of long-term bedrock incision efficiency by short-term alluvial
893 cover intermittency, *J. Geophys. Res.*, 115, doi:10.1029/2008JF001210.

894 Lague, D. (2014), The stream power river incision model: evidence, theory and beyond, *Earth*
895 *Surf. Process. Landforms*, 39(1), 38–61, doi:10.1002/esp.3462.

896 Lamb, M. P., W. E. Dietrich, and L. S. Sklar (2008), A model for fluvial bedrock incision by
897 impacting suspended and bed load sediment, *J. Geophys. Res.*, 113(F3), F03025,
898 doi:10.1029/2007JF000915.

899 Lamb, M. P., N. J. Finnegan, J. S. Scheingross, and L. S. Sklar (2015), New insights into the
900 mechanics of fluvial bedrock erosion through flume experiments and theory,
901 *Geomorphology*, 244, 33–55, doi:10.1016/j.geomorph.2015.03.003.

902 Lisle, T. E., and M. Church (2002), Sediment transport-storage relations for degrading, gravel
903 bed channels, *Water Resour. Res.*, 38(11), doi:10.1029/2001WR001086.

904 Montgomery, D. R., and J. M. Buffington (1997), Channel-reach morphology in mountain
905 drainage basins, *Geol. Soc. Am. Bull.*, 109(5), 596–611, doi:10.1130/0016-
906 7606(1997)109<0596:CRMIMD>2.3.CO;2.

907 Nelson, P. A., M. B. Pittaluga, and G. Seminara (2014), Finite amplitude bars in mixed
908 bedrock-alluvial Channels, *J. Geophys. Res. Earth Surf.*, 119, 566–58,
909 doi:10.1002/2013JF002957.

910 Nelson, P. A., and G. Seminara (2011), Modeling the evolution of bedrock channel shape
911 with erosion from saltating bed load, *Geophys. Res. Lett.*, 38(17), L17406,
912 doi:10.1029/2011GL048628.

913 Nelson, P. A., and G. Seminara (2012), A theoretical framework for the morphodynamics of
914 bedrock channels, *Geophys. Res. Lett.*, 39, L06408, doi:201210.1029/2011GL050806.

915 Nittrouer, J. A., D. Mohrig, M. A. Allison, and A.-P. B. Peyret (2011), The lowermost
916 Mississippi River: a mixed bedrock-alluvial channel, *Sedimentology*, 58(7), 1914–1934,
917 doi:10.1111/j.1365-3091.2011.01245.x.

918 O'Connor, J. E., J. F. Mangano, S. W. Anderson, J. R. Wallick, K. L. Jones, and M. K. Keith
919 (2014), Geologic and physiographic controls on bed-material yield, transport, and channel
920 morphology for alluvial and bedrock rivers, western Oregon, *Geol. Soc. Am. Bull.*,
921 B30831.1, doi:10.1130/B30831.1.

- 922 Pyrcce, R. S., and P. E. Ashmore (2003), The relation between particle path length
923 distributions and channel morphology in gravel-bed streams: a synthesis, *Geomorphology*,
924 56(1-2), 167–187, doi:10.1016/S0169-555X(03)00077-1.
- 925 Richardson, K., and P. A. Carling (2005), A typology of sculpted forms in open bedrock
926 channels, *Geological Society of America Special Papers*, 392, 1–108, doi:10.1130/0-8137-
927 2392-2.1.
- 928 Scheingross, J. S., F. Brun, D. Y. Lo, K. Omerdin, and M. P. Lamb (2014), Experimental
929 evidence for fluvial bedrock incision by suspended and bedload sediment, *Geology*,
930 G35432.1, doi:10.1130/G35432.1.
- 931 Sklar, L. S., and W. E. Dietrich (2004), A mechanistic model for river incision into bedrock
932 by saltating bed load, *Water Resour. Res.*, 40, W06301, doi:10.1029/2003WR002496.
- 933 Tinkler, K., and E. Wohl (1998), A Primer on Bedrock Channels, in *Rivers Over Rock:
934 Fluvial Processes in Bedrock Channels*, edited by K. J. Tinkler and E. E. Wohl, pp. 1–18,
935 American Geophysical Union.
- 936 Turowski, J. M., A. Badoux, J. Leuzinger, and R. Heggin (2012), Large floods, alluvial
937 overprint, and bedrock erosion, *Earth Surf. Process. Landforms*, 38, 947–958,
938 doi:10.1002/esp.3341.
- 939 Turowski, J. M., N. Hovius, H. Meng-Long, D. Lague, and C. Men-Chiang (2008),
940 Distribution of erosion across bedrock channels, *Earth Surf. Process. Landforms*, 33(3), 353–
941 363, doi:10.1002/esp.1559.
- 942 Whitbread, K., J. Jansen, P. Bishop, and M. Attal (2015), Substrate, sediment, and slope
943 controls on bedrock channel geometry in postglacial streams. *J. Geophys. Res. Earth Surf.*,
944 120, 779–798. doi: 10.1002/2014JF003295.
- 945 Wohl, E. E., and D. M. Merritt (2001), Bedrock channel morphology, *Geol. Soc. Am. Bull.*,
946 113(9), 1205–1212.
- 947 Yanites, B. J., and G. E. Tucker (2010), Controls and limits on bedrock channel geometry, *J.*
948 *Geophys. Res.*, 115(F4), F04019, doi:10.1029/2009JF001601.